Equal Channel Angular Processing of Polymers

by

Omar Kheir

A thesis submitted in partial fulfillment
of the requirements for the degree of
Master of Science in Engineering
(Industrial and Systems Engineering)
in the University of Michigan-Dearborn
2019

Master's Thesis Committee:

Assistant Professor Georges Ayoub, Chair
Professor Ghassan Kridli
Assistant Professor Abdallah Chehade

Dedication

This dissertation is dedicated to all those who supported me throughout this journey, especially my parents and sister.

Acknowledgements

Foremost, I would like to thank Prof. Georges Ayoub for his continuous support and daily guidance throughout my master's coursework and research at UM-Dearborn, for his patience and motivation and for offering me this life-changing opportunity.

I want to express my gratitude to Prof. Ghassan Kridli who served as my co-advisor and for the support over the past couple of years.

Finally, I would like to thank Prof. Abdallah Chehade and Prof. Ghassan Kridli for serving on my thesis committee.

Table of Contents

List of Tables

List of Figures

Abstract

Polyethylene is a polymeric material that has a wide variability in its crystal content covering a broad range of mechanical properties. Equal Channel Angular Processing (ECAP) is a severe plastic deformation technique used to alter the material's mechanical properties. In this study, the effect of ECAP on the different crystallinities of polyethylene was studied, namely; high-density polyethylene (HDPE) and low-density polyethylene (LDPE). A full-factorial experimental design was adopted for the ECAP experiments at two main extrusion rates (4.5 and 45mm/min) and four different back-pressures (0, 375, 745 and 1120N). Two repetitions of each ECAP extrusion condition were performed. After ECAP, tensile test coupons were machined from the processed material. The tensile specimens were then tested at two different strain rates: 2.58 and 25.8mm/min. The test results were used to evaluate the effects of back-pressure, extrusion velocity and strain rate on the yield strength and the total strain to failure. Compared with the as-received materials, the results showed that increasing the back-pressure led to a decrease in both the yield strength and the modulus of elasticity for the processed materials. The total strain to fracture showed an increase for the processed LDPE material with the increase of the back-pressure, but a decrease was observed in the total strain to fracture for the HDPE material. When comparing the properties of the ECAP-processed PE the following was observed: an increase of the extrusion velocity had opposite effects for the LDPE compared to the HDPE. The yield strength, the total strain to fracture and the modulus of elasticity increased for the processed LDPE

material with the increase of the extrusion velocity while all of these properties decreased for the HDPE.

Chapter 1
Introduction

Two different types of polymers exist: semi-crystalline and amorphous. In this work, the effort is focused on studying semi-crystalline polymers. Semi-crystalline polymers have been widely used in different applications in many fields that include but not limited to the automotive industry, electronics and biomedical devices. Polymers are starting to replace metals in numerous application due to their lower cost, weight and satisfactory properties (Makki et al., 2017). The variable morphology of semi-crystalline polymers allows a wide range of applications due to the ability of having different mechanical properties such as in tissue engineering, food packaging industry, aerospace, sports equipment and 3D printing. A change in the mechanical response is possible by changing the mechanical properties through the control of the processing variables of the semi-crystalline polymers such as the molecular weight, chain length distribution, degree of crystallinity and the addition of copolymers or ionomers (Peacock, 2000). Unlike other materials, such as metals and ceramics that are formed by atoms or ions, polymers are formed by a chain of molecules known as macromolecules which are mostly organic in origin, composed of hydrocarbons and nonmetallic elements. Semi-crystalline polymers have low electrical conductivities, are non-magnetic and chemically inert. The use of semi-crystalline polymers strongly depends on improving and understanding their mechanical behavior through severe deformation processes. This chapter is mainly concerned with the physical, chemical structure and mechanical behavior of semi-crystalline polymers, specifically polyethylene as well as the concept

of equal channel angular processing (ECAP) followed by the different work done on ECAP for polymers.

1.1. Semi-crystalline Polymers

The word "Polymers" is composed of two Greek words: "Poly", meaning many, and "mer", meaning unit. Therefore, a polymeric molecule is a macromolecule consisting of repetitive units which are chemically joined. The polyethylene monomer unit is C_2H_4 of which the chains are composed from hundreds or even millions of these units (Young, 1981). The core of the molecular chain is a string of carbon atoms that are connected to each other and to hydrogen atoms since the carbon atoms have 4 available electrons for covalent bonds (Figure 1.1).

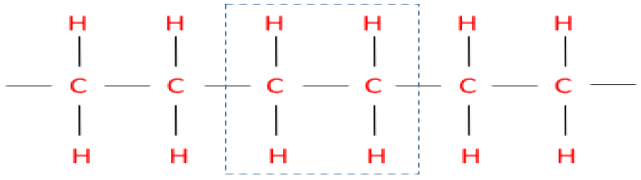

Figure 1.1: Polyethylene chain formed from monomer units (dashed box).

Intermolecular bonds also exist, knows as the van der Waals which are weaker than covalent bonds and mostly dependent on the masses and distances of the molecules.

1.1.1. Polymerization

Polymers are created through the polymerization chemical reaction which joins the different monomers together, forming a large chain. Obtaining polyethylene is usually initiated by adding a catalyst to ethylene monomers and by providing the appropriate temperature and pressure.

A commonly used catalyst is peroxide (R_2O_2) that reacts with the monomer, forming pairs of free radicals. The double bonds in the ethylene molecules break up and the two free electrons would be used to connect the carbon atoms to other monomers. Termination would happen when, at the end of the chain, two of the radicals pair up. When polymers are formed of only one type of monomers, they are called homopolymers such as polyethylene, while polymers that are composed of more than one type of monomers are referred to as copolymers (Peacock, 2000).

1.1.2. Molecular Shape

Polymeric chains are three-dimensional due to their ability to rotate and bend. Three carbon atoms are shown in Figure 1.2 where the third atom lies on the cone of revolution at a 109^0 angle. Bending, twisting and kinks would then be present in those single chain molecules causing intertwining and entanglement with the neighboring chains due to this three-dimensional geometry. A single chain molecule is shown in Figure 1.3 exhibiting random kinks and coils.

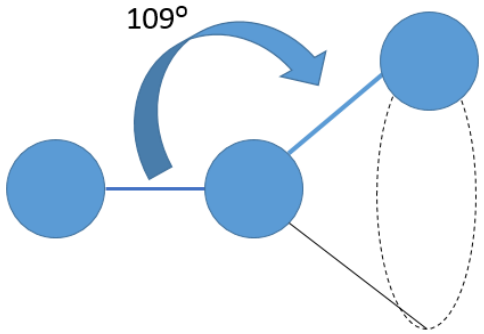

Figure 1.2: Carbon-Carbon covalent bonding.

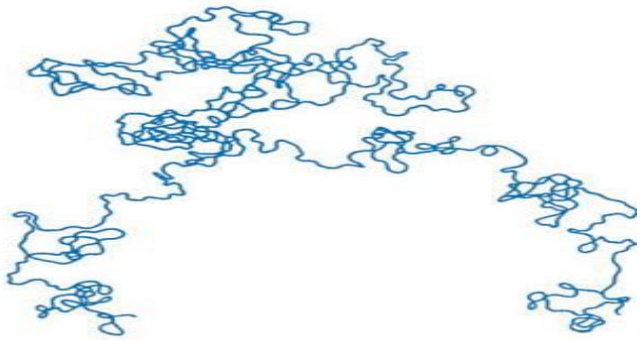

Figure 1.3: Single polymer chain molecule with twisting and kinks.

1.1.3. Chemical Structure

The polymerization conditions (pressure, temperature and catalyst) of polyethylene affect the way monomers are arranged along the chain as shown in Figure 1.4, resulting in either a linear setup, branched cross-linked or in a network. In the case of linear polymers, monomers are joined along a single chain without having any type of side attachments. Hydrogen and van der Waals exist between the chains. Branched polymers have side branches that are due to side reactions occurring during the synthesis of the polymers and are connected to the main chain. When a hydrogen atom is replaced by a covalently bonded polyethylene chain, branching occurs while crosslinking occurs by having additive atoms or molecules that get attached to the chain through covalent bonds forming a network. The chains in cross-linked polymers are interconnected through adjacent chains (Horie et al., 2004). Finally, network polymers are three dimensional networks due to monomers having three or more active covalent bonds (Jenkins et al., 1996).

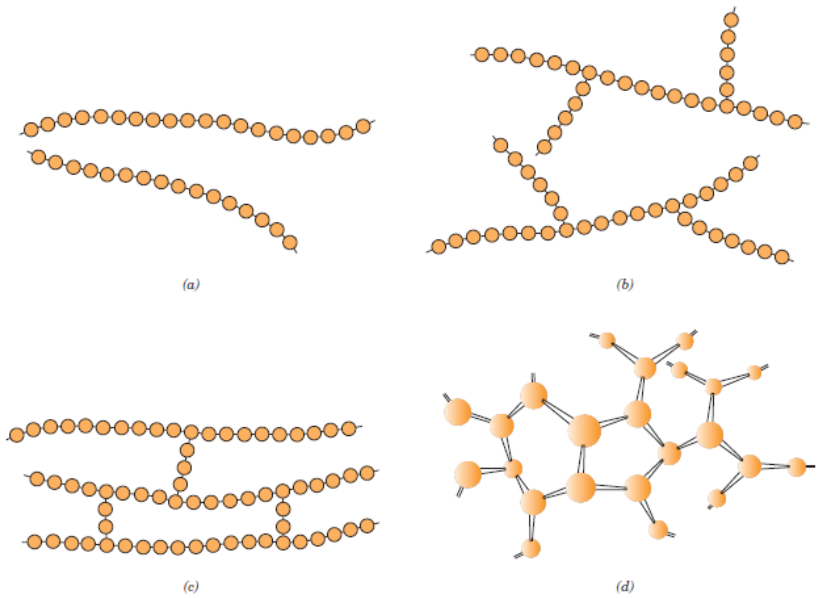

Figure 1.4: Molecular structures in semi-crystalline polymers
(a) linear, (b) branched, (c) cross-linked, (d) network (Callister, 1997).

1.1.4. Crystallinity in Polymers

Semi-crystalline polymers are characterized by having a complex morphology and are known to be heterogeneous materials as they are composed of two distinct phases: the crystalline phase which consists of ordered molecular arrangements while in the amorphous phase, the chains are randomly ordered. This heterogeneity differentiates semi-crystalline polymers from metals and ceramics as they are either completely crystalline or non-crystalline. The rate of solidification is the main factor affecting the crystal content in semi-crystalline polymers which can range anywhere from 5% to 95% (Bartczak and Galeski, 2010a).

1.1.4.1. Crystalline Phase

Orthorhombic or monoclinic unit cells form the crystalline phase in which the chain segments of the molecules are packed in arrays (Lin and Argon, 1994). A unit cell for polyethylene of an orthorhombic geometry is shown in Figure 1.5. The lattice parameters of the orthorhombic unit cell are as follows: a=7.42 Å, b=4.94 Å and c=2.5 Å, where c is parallel to the axis of the chain. The segments of the chains are connected through covalent bonds which are parallel to the c-axis while weaker bonds exist between the chains, known as the van der Waals bonds. These unit cells would be joined together in order to form crystallites having a precise alignment. The orderly-shaped crystals are called lamellae and have a thickness that ranges between 20 to 170 Å.

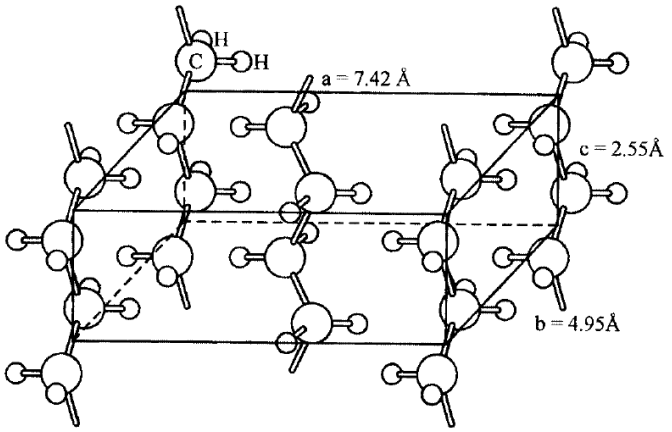

Figure 1.5: Orthorhombic unit cell of polyethylene (Peacock, 2000).

1.1.4.2. Amorphous Phase

In the amorphous phase, the chains are disorderly organized. Figure 1.6 shows the segments where a crystallite crosses the amorphous phase and connects to another crystallite forming “tie chains”, or instead, end without connecting or returning to anything, or form “loops” that return to where they came from, or finally, entangled loops where two crystallites are

interconnected (Peacock, 2000). The crystallization process, the molecular weight and branching are all factors affecting the ratio of the loops versus cilia chains.

Figure 1.6: Tie chains, cilia, loops and entangled loops from left to right respectively.

1.1.5. Spherulitic Structure

A spherulitic, spherical-structured, shape is formed in semi-crystalline polymers such as polyethylene which are crystallized from melt. Many spherulites form the semi-crystalline polymers that are separated through interspherulitic boundaries as shown in Figure 1.7. Both of the crystalline and amorphous phases are connected through covalent bonds of the polymeric chains as referred to earlier in Figure 1.6, such as the tie chains. These tie chains block the separation of the amorphous and crystalline phases when subjected to loading (Brown and Ward, 1983).

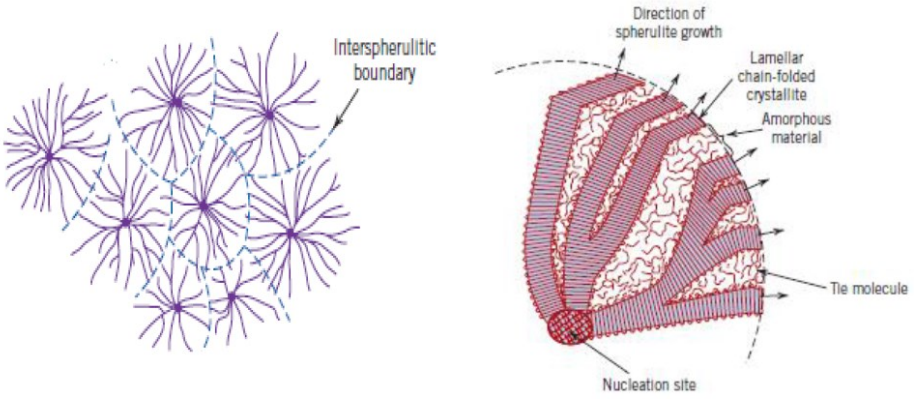

Figure 1.7: Semi-crystalline polymers microstructure (Callister, 1997).

1.1.6. Mechanical Behavior

Due to the semi-crystalline structure, polymers can exhibit a wide range of mechanical behavior. A true stress-strain curve for high density polyethylene is shown in Figure 1.8 under uniaxial tension at room temperature conditions. The deformation behavior of high density polyethylene occurs as follows: a linear elastic region at the beginning, a gradual increase in the stress after yielding followed by rapid increase in the stress until failure. Furthermore, the mechanical behaviors of three different types of polyethylene with different crystal content are shown in Figure 1.8. The crystal content is not the only factor affecting the mechanical behavior of semi-crystalline polymer, factors such as the molecular weight, chain length distribution, cross-linking, the size, shape and orientation of the lamellae also affect the mechanical behavior. The temperature, strain rate and loading direction are additional factors affecting the mechanical behavior (such as the Young's modulus, yield stress, ductility and strain hardening). The temperature drastically affects the behavior of semi-crystalline polymers: at low temperatures, they could exhibit a glass-like brittle behavior and as the temperature increases, the Young's modulus decreases (along with the yield stress and strain hardening) rendering the material more ductile

leading to a rubber-like behavior at high temperatures (Brooks et al., 1998; Pampillo and Davis, 1972a). The rate of deformation is also main factor affecting the behavior of semi-crystalline polymers: the higher the strain rate, the higher the yield stress, plastic flow and the strain hardening would be (Ayoub et al., 2011a). The anisotropic nature of the material makes it sensitive to the loading path (Hachour et al., 2014a).

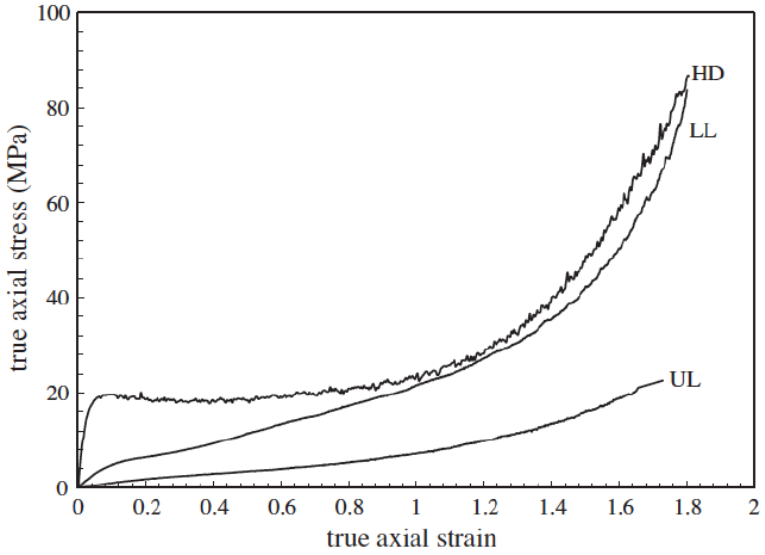

Figure 1.8: Stress-strain response of PE materials; (HD) High density polyethylene, (LL) Low density polyethylene, (UL) Ultra-low density polyethylene (Ayoub et al., 2010).

1.1.6.1. Semi-crystalline polymers deformation

The complex morphology of semi-crystalline polymers results in a complex deformation mechanism that occurs at multiple stages. Under a uniaxial tensile test, the deformation could be characterized into four main steps, also shown in Figure 1.9:

- The amorphous chains elongate and the weak bonds between them break
- The crystalline lamellae re-orient and rotate in the same direction of the applied load.

- The lamellae would then tilt and the adjacent chains would slide resulting into the fragmentation of those lamellae into crystalline blocks. The van der Waals bonds would resist the deformation.
- The new blocks would then align in the maximized direction of stretch, disintegrating themselves into a fibrillary structure.

This deformation would result in decreasing the distance between the chains, therefore, increasing the entanglements which causes strain hardening in the deformed polymer.

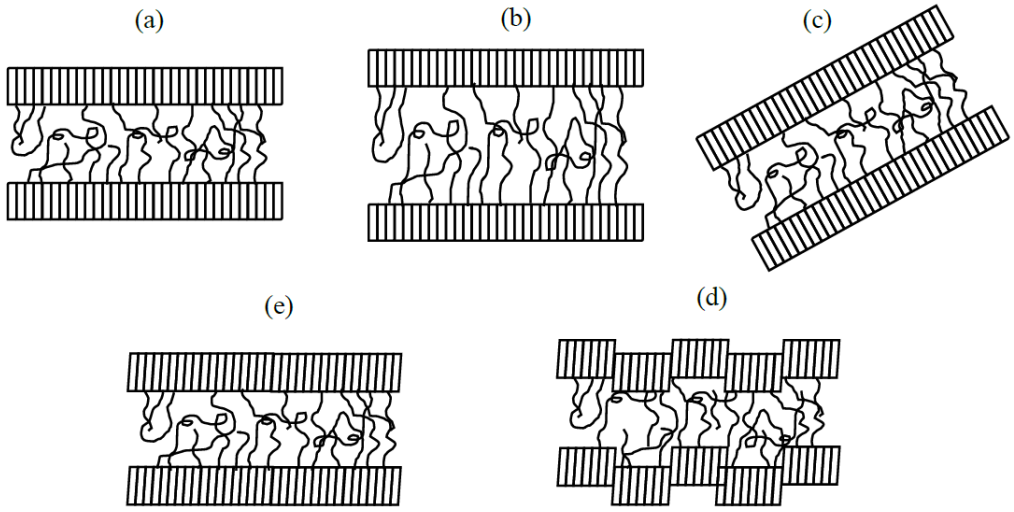

Figure 1.9: Inter and intra-lamellar deformation, a) before deformation, b) elastic deformation: elongation of amorphous chains, c) elastic deformation: inter-lamellar rotation, d) plastic deformation: tilting of lamellas, e) plastic deformation: fragmentation of the lamella.

1.2. Equal Channel Angular Processing

The processing of materials through Severe Plastic Deformation (SPD) dates back to ancient times. Some of the SPD techniques that were introduced included conventional Equal Channel Angular Processing (ECAP), developed ECAP processes, accumulative roll-bonding and

high-pressure torsion. They have become a major part of the materials processing field that aims at improving the mechanical properties of a certain material. Our knowledge of those different deformation techniques has been continuously improving although the developments of the SPD techniques are still at their initial stages (Vladimir M. Segal, 2017). The first bulk material that was processed by SPD was produced in 1971 that demonstrated a higher strength and an improved ductility.

In the literature, one of the most commonly used Severe Plastic Deformation processes is Equal Channel Angular Processing (ECAE) which could be found under different names: ECAE (extrusion), ECAF (forging), ECAR (rolling). The introduction of ECAP goes back to the early 70s by Vladimir M. Segal. Segal's involvement in different projects made him realize the lack of 'ideal' deformation mode to enhance the properties of a certain material. The efforts leading to the development of the ECAP involved imposing a simple shear deformation through a "cross-extrusion" process as shown in Figure 1.10 (V. A. Beloshenko et al., 2013; M. Furukawa et al., 2001; Valiev and Langdon, 2006).

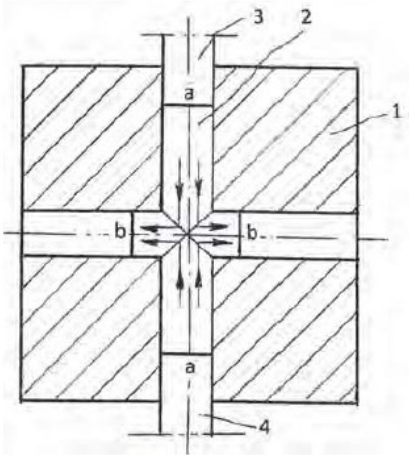

Figure 1.10: Simple shear in cross-extrusion (Vladimir M. Segal, 2017).

1.2.1. Principle of ECAP

Unlike the conventional methods such as rolling and extrusion, ECAP does not result into a change in the dimensional properties of the processed sample (M Furukawa et al., 2001).

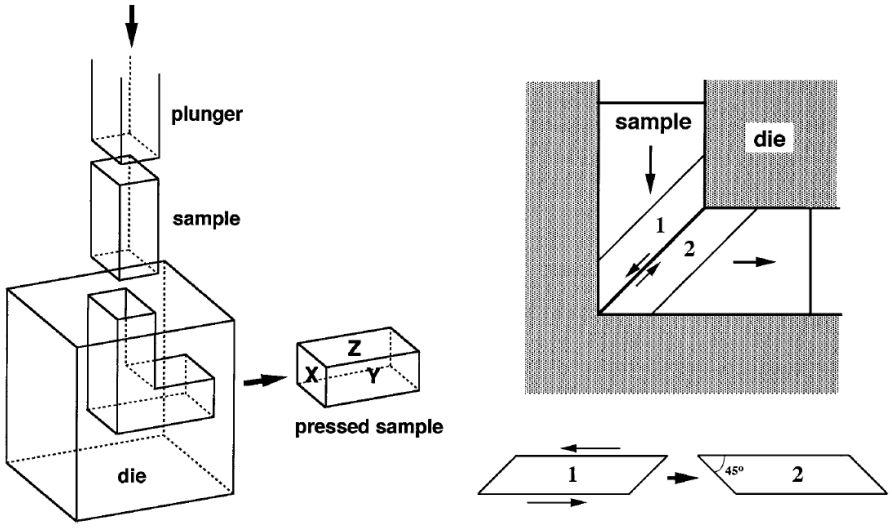

Figure 1.11: Illustration of the ECAP process (M Furukawa et al., 2001).

A schematic representation of the ECAP setup is shown in Figure 1.11 which consists of a die having two inner channels of equal cross-sections and intersecting at a certain angle that could be variable. The sample is specifically prepared to fit in these channels and is pressed through the die at a constant rate. As the sample is pushed through the die, the strain is imposed as shown in Figure 1.11 resulting in simple shear between the '1' and '2' segments shown (M Furukawa et al., 2001). Figure 1.11 also shows three different planes that were defined for the sample at the exit of the die where the "x" plane is perpendicular to the direction of the movement of the sample.

A sectional view of the ECAP die is shown in Figure 1.12 where the two critical design angles Φ and Ψ are represented. Φ represents the angle between the channels while Ψ represents

the outer curvature arc. The value of the angles of Φ and Ψ are two main factors affecting the value of the von Mises equivalent strain.

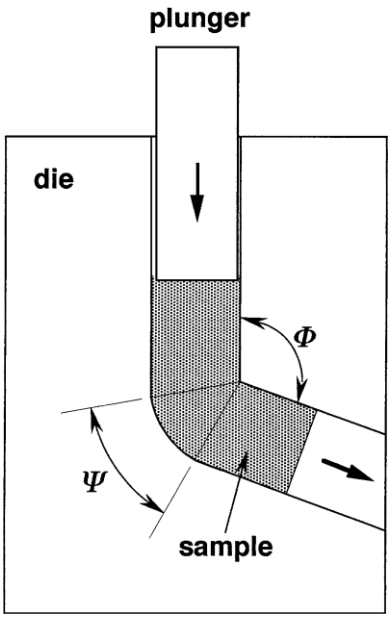

Figure 1.12: A sectional view of the ECAP die showing the critical design angles (M Furukawa et al., 2001).

1.2.2. Experimental factors influencing ECAP

Three main types of experimental factors could be found: the factors that are linked directly to the setup of the ECAP such as the angles of the channel and the curvature; the factors that are dependent on the experimentalist such as the pressing speed, temperature and back-pressure; the factors affecting the grain refinement and microstructure which are the different processing routes (M Furukawa et al., 2001; Furukawa et al., 2003; Valiev and Langdon, 2006).

1.2.2.1. Influence of the channel angle ∅

The channel angle controls the level of strain imposed on the processed sample. Most experimental results have been reported with channel angles of the die ranging between ∅ = 90° and 120° and there are only very few comparisons between the different results obtained from different angles. Nakashima et al., 1998 conducted experiments on four sets of dies with angles ranging from 90° to 157.5° and Huang et al., 2001 compared a 90° angle channel with a 120° channel. Experiments have shown that the more intense the plastic strain (i.e. the lower the angle), the more uniform the microstructure and the more refined the grains would be.

1.2.2.2. Influence of the angle of curvature Ψ

The intersection of the outer parts of the channel within the die represents the angle of curvature Ψ. This angle has a minor effect on the strain imposed on the sample although it does influence the production of ultra-grained materials. There have been several studies to analyze the effect of the curvature angle Ψ in ECAP (Bowen et al., 2000; Chung et al., 2004; DeLo and Semiatin, 1999; Kim et al., 2001; Lee et al., 2004; Park and Suh, 2001; Pei et al., 2003; Prangnell et al., 1997; Semiatin et al., 2000). The goal behind the angle of the curvature was to prevent the occurrence of the "dead zones" where the sample would not remain in contact with the outer corner of the die. For practical reasons, ECAP dies are usually designed with a Ψ of around 20° (Valiev and Langdon, 2006). Figure 1.13 illustrates the concept of the angle of curvature Ψ along with the channel angle ∅.

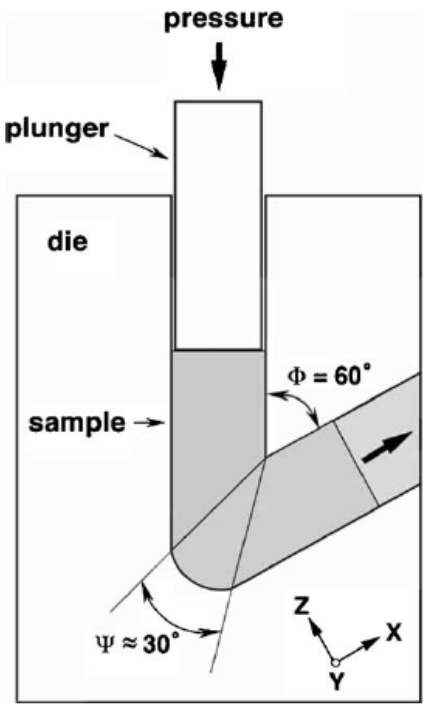

Figure 1.13: Illustration of an ECAE die showing the different channel and curvature angles (Furuno et al., 2004).

1.2.2.3. Influence of the pressing speed

Typical pressing speeds that have been used during ECAP experiments range between 1-20 $mm.s^{-1}$ through either high-capacity hydraulic presses or conventional mechanical testing machines. The effect of the pressing speed on pure aluminum samples on speeds ranging from 10^{-2} to 10 $mm.s^{-1}$ was investigated (Berbon et al., 1999a; Kim et al., 2003). The results have shown that no significant influence was detected on the size of ultrafine grains but easier recovery is reached at lowers speeds. Abrupt heating was detected at higher rates while no heating was detected at slower rates (Yamaguchi et al., 1999).

1.2.2.4. Influence of the pressing temperature

The pressing temperature during ECAP could be controlled easily, by processing the material in a heated die. Experimental results have shown that as the temperature increases, the grain size tends to increase (Yamashita et al., 2000). Although it is generally easier to process specimens at high temperatures, ultra-fine grained microstructures are generally achieved under the lowest possible temperatures (Chen et al., 2003; Huang et al., 2004; Shin et al., 2002).

The higher the strength of the sample material used in ECAP or the higher the ram speed is, the higher the temperature rise would be.

1.2.2.5. Influence of back-pressure

The concept of back-pressure was introduced in the early discovery of the ECAE process although it has not been applied until recently due to the improvement of the ECAE design as well as the ability to have a precise computer-controlled back-pressure. The importance of the back-pressure lies in the improvement of the workability of the samples (Valiev and Langdon, 2006) as well as the physical enhancement and better preservation of the initial cross-sectional shape of the sample improving the uniformity of the microstructure (Semiatin et al., 2000). Figure 1.14 illustrates the concept of the back-pressure.

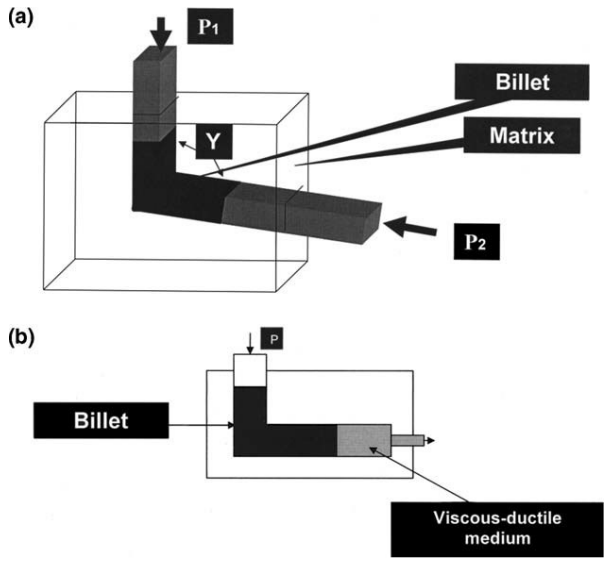

Figure 1.14: Illustration of the ECAP with back-pressure (Valiev and Langdon, 2006).

1.2.3. Fundamental Parameters in ECAP

1.2.3.1. Strain imposed in ECAP

A strain is imposed on the sample processed through the ECAP die. The estimation of the strain is done analytically through the 2-D illustrations shown in Figure 1.15. $\emptyset$ being the channel angle and Ψ the angle of curvature (Iwahashi et al., 1996). Figure 1.15(a) represents the case where $\Psi = 0^o$, Figure 1.15(b) represents $\Psi = (\pi - \emptyset)^o$ and (c) $0^o < \Psi < (\pi - \emptyset)^o$. We assume in this case that friction is negligible in the die if the specimen was well-lubricated.

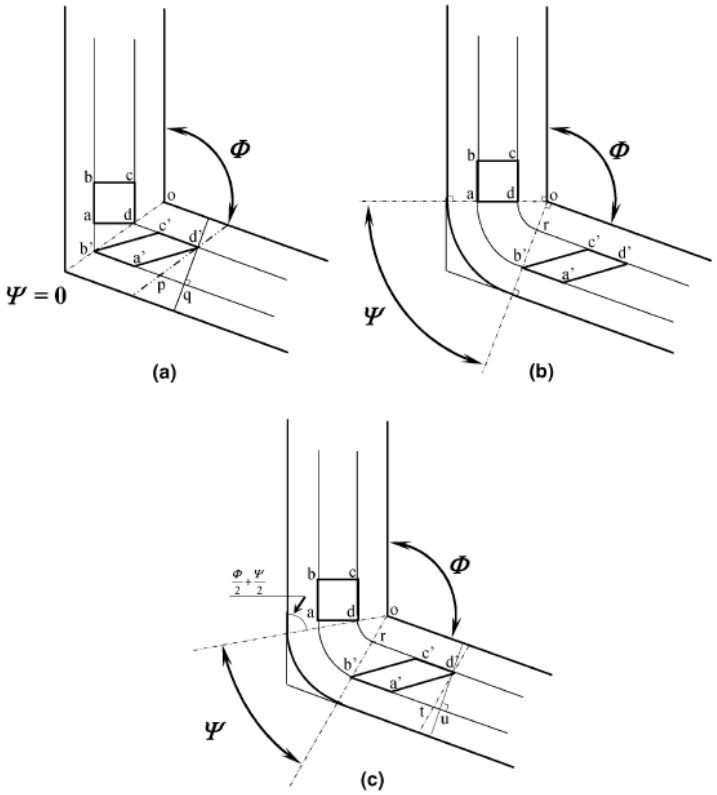

Figure 1.15: The 3 different design configurations for the ECAP channel (a) Ψ = 0°, (b) Ψ = ($\pi - \emptyset$)° , (c) 0° < Ψ < ($\pi - \emptyset$)° (Iwahashi et al., 1996).

Using purely the geometrical properties of Figure 1.15(a), we can conclude that the shear strain γ is:

$$\gamma = 2\cot\left(\frac{\phi}{2}\right) \qquad (1.1)$$

The shear strain for Figure 1.15(b) is $\gamma = \Psi$ and the shear strain of Figure 1.15(c) is:

$$\gamma = 2\cot\left(\frac{\phi}{2}+\frac{\Psi}{2}\right) + \Psi\,\mathrm{cosec}\left(\frac{\phi}{2}+\frac{\Psi}{2}\right) \qquad (1.2)$$

The previous equation could be reduced to that of Figure 1.15(a) if Ψ = 0° and it could be reduced to that of Figure 1.15(b) if Ψ = ($\pi - \emptyset$)°.

After N passes through the ECAP die, the equivalent strain expression is given by (Iwahashi et al., 1996):

$$\varepsilon_N = \frac{N}{\sqrt{3}}\left[2\cot\left(\frac{\phi}{2}+\frac{\Psi}{2}\right) + \Psi\,\mathrm{cosec}\left(\frac{\phi}{2}+\frac{\Psi}{2}\right)\right] \quad (1.3)$$

The equivalent strain equation has been proven to be applicable through experiments that been conducted through layers of colored plasticine and half-billets of aluminum that had a rectangular grid drawn on it (Shan et al., 1999).

1.2.4. The processing routes in ECAP

There are four possible routes to follow when processing a sample through an ECAP die by changing its rotation between the individual pressings (Furukawa et al., 2003; Horita et al., 2000). The possible routes (shown in Figure 1.16) are:

- Route A: the sample is not rotated between the different pressings.
- Route BA/BC: the sample is rotated by 90º between the pressings either in the same or opposite directions.
- Route C: the sample is rotated by 180º between the pressings.

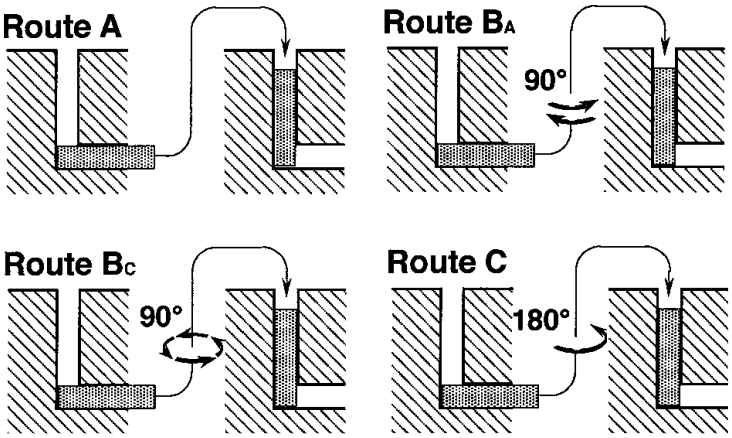

Figure 1.16: The different routes for multiple pressings (M Furukawa et al., 2001).

Route B could be executed in two different ways, either by rotating the sample between the pressings in the same direction by 90° (called route BA) or by rotating the sample by 90° between the pressings in opposite directions each time (called route (BC) as illustrated in Figure 1.16.

Experimental results have shown that no improvement is achieved through the more complex routes BC and C. The predictions presented through the illustrations in Figure 1.17 were confirmed through experimental tests on pure Aluminum samples through optical microscopy (Iwahashi et al., 1998).

1.2.4.1. Effects of the processing routes

The different shear planes of each processing route are shown in Figure 1.17 for multiple passes and across the X, Y and Z planes. We consider an ECAP die with $\Psi = 0^{o}$ with $\Phi = 90^{o}$. For route C, the shearing remains on the same plane between the passes while the direction alternates which means that route C is redundant after even number of passes. The same applies

to route BC as well because 4 passes would constitute a complete cycle through which the sample would go through a redundant strain process.

Routes A and BA are not redundant where a cumulative build-up of strain is proven to occur after multiple passes.

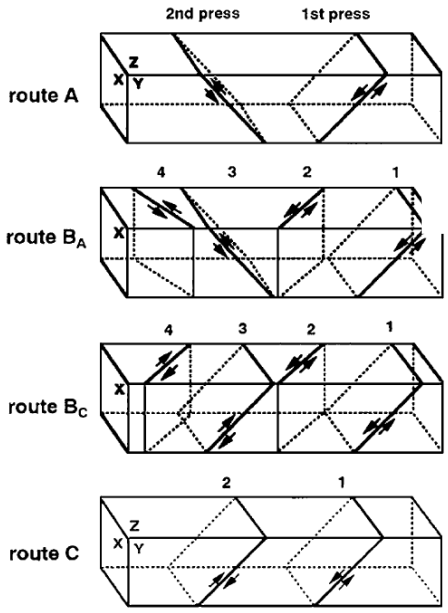

Figure 1.17: The different slip systems on the X, Y, Z planes for the consecutive and the different types of passes (M Furukawa et al., 2001).

Figure 1.18 shows the different shearing patterns through planar cross-sections of a 90º ECAP die using the 4 different processing routes. The illustrations show the macroscopic distortions resulting from the process. The figure proves once again that the original cubic shape of the element is restored after 2 passes for route C and after 4 passes for route BC. Routes A and BA have shown larger distortions as the number of passes increased.

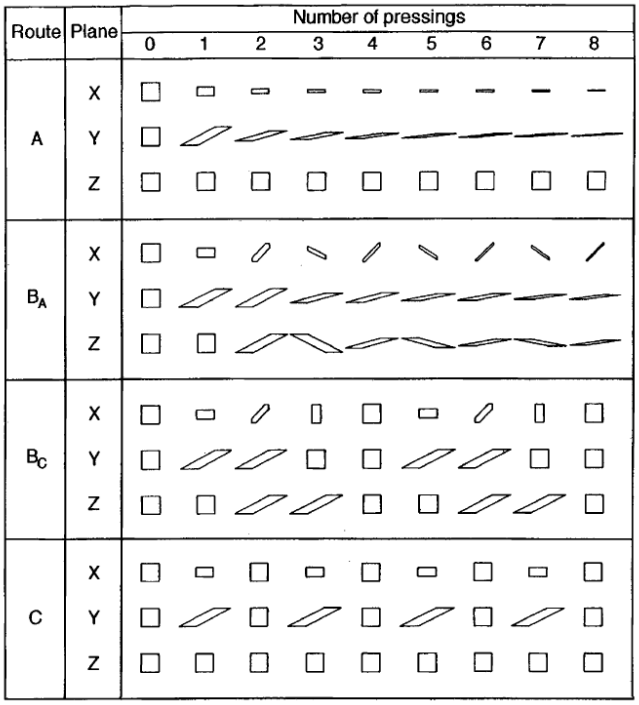

Figure 1.18: The distortions along the X, Y and Z planes after each pass of the different processing routes.

Each route leads to different results for the macroscopic grains. Route A leads to the elongation of the grains along the same plane (y-plane) while route B results in the elongation of the grains along both orthogonal x and y planes.

In conclusion, when having more than two passes, routes A and BA lead to the similar effects by increasing the distortion of the original cubic element while routes C and BC are similar to each other and contribute to the restoration of the cubic elements after 2n and 4n passes respectively for these routes.

1.2.5. Microstructural characteristics of ECAP

The investigation of the microstructure was achieved through different experiments conducted on polycrystalline material through the ECAP and its different processing routes

(Gholinia et al., 2000; Iwahashi et al., 1998). The main effect of ECAP is the significant grain refinement even after only one pressing through the die. It has been proven that the refinement of grains during the ECAP process is independent of the speed of pressing (Berbon et al., 1999b). The microstructure of the sample after ECAP depends on the processing route. In the case of the die with an internal angle of 90°, the most optimal processing route is BC. Experimental results also suggest that route A is more effective in dies with an angle of 120° which is due to the change of the shearing plane's interaction with the deformation texture. The pressing process and the numbers of passes are critical elements in order to achieve a stable grain size and a homogeneous microstructure. An ultrafine microstructure of a pure aluminum sample is shown in Figure 1.19 that has been processed four times through an ECAP die using a BC route (Iwahashi et al., 1998). The average grain size was reduced from ~1.0 mm after annealing before ECAP to ~1.3 μm after ECAP.

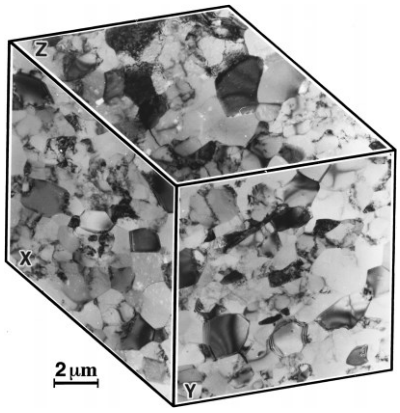

Figure 1.19: The microstructure of an Aluminum ECAP-processed sample after 4 passes (Iwahashi et al., 1998)

1.2.6. ECAP of Sheets

The use of ultrafine-grained materials in some industrial applications has to be necessarily in the form of thin sheets. This has created the need to apply ECAP to bulk sheets

where the output material could be directly used in the manufacturing processes (Valiev and Langdon, 2006). Only a few studies have been conducted on the application of ECAP to sheets (Ferrasse et al., 2008; Kamachi et al., 2003; Sue et al., 1999; Suh et al., 2015).

There are mainly two different configurations to press the plate samples: a vertical configuration or a horizontal configuration as shown in Figure 1.20. All the mentioned studies, have been conducted in the horizontal configuration due to its practicality.

1.2.6.1. Processing routes for plate samples

Unlike the case of billets and rods, the geometry of the plates presents different possible rotations between passes.

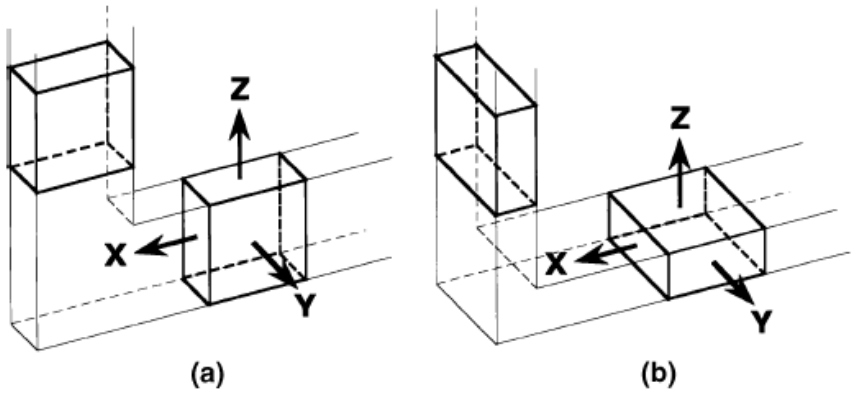

Figure 1.20: Possible configurations to press the ECAP plates through the die: (a) vertical configuration (b) horizontal configuration (Kamachi et al., 2003)

The rotations along the X axis and Y axis are now limited to 180° rotations only while rotations along the Z axis could be of 90° as shown in Figure 1.21. A 180° rotation around the X axis is called route C_X which is the same as route C for rods and bar samples while a 180° rotation around the Y axis is called route C_Y and is equivalent to route A for bars and samples. Additional

routes are available for plate samples involving rotations around the Z axis by 90°, creating routes BAZ and BCZ, where each sample is rotated by 90° between the passes in opposite directions or the same direction, respectively. Experimental results on aluminum plates have shown that route BCZ leads to great properties and only has minor inhomogeneity after 4 passes (Kamachi et al., 2003).

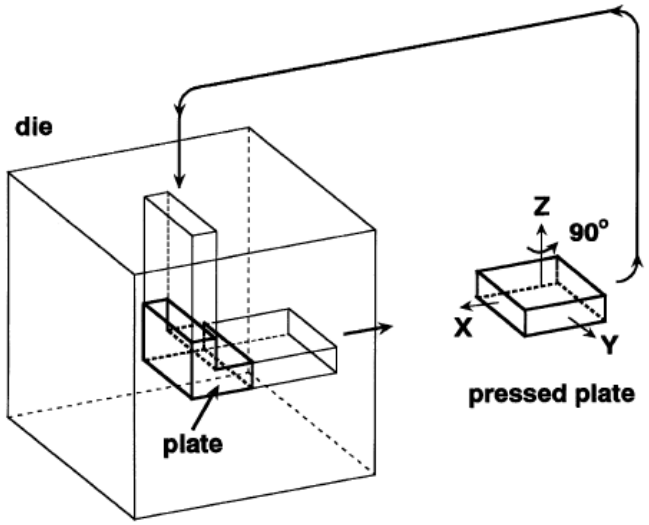

Figure 1.21: Processing routes of the ECAP of plates (Kamachi et al., 2003).

1.3. ECAP of Polymers

The ECAP process was originally invented for crystalline materials in the early 70s with more than 200 papers published yearly about the ECAP of metals while the polymeric materials have not received as much attention. ECAP is utilized in order to form an oriented microstructure promoting higher directional strength characteristics. ECAP was not applied to polymers until the late 90s where the studies were mostly focused on investigating the microstructure, the properties of the processed samples and the texture development (Bouaksa et al., 2014; Boulahia et al., 2009; Perig et al., 2010; Perig and Golodenko, 2014).

1.3.1. Types of processed polymers

- **Monolithic billet**

One pass of ECAE was enough to determine that the low-density polyethylene (LDPE) with a route A, Φ=90°, provides an oriented formation of the material at room temperature. After two passes, the spherulites were destructed and after four passes, the ECAP process transformed those spherulites into stacks of crystalline lamellae which are aligned with the direction of the extrusion (Sue and K.-Y.Li, 1998). A similar case was identified by Bartczak et al., 1994 for the ECAP of high density polyethylene (HDPE). In most of the cases, the ECAP experiments are executed at room temperature and a mechanical destruction occurs due to cold deformations. The process results in a lower crystallinity and density but increases the mechanical properties of the material. For example one pass of ECAP, increased the modulus of elasticity at tension E from 2.89GPa to 3.47GPa, when the sample is cut in the direction of the extrusion while in the transversal direction, the modulus of elasticity is reduced to 2.66GPa (Wang et al., 2011).

- **Powder billet**

ECAP, coupled with back-pressure, is commonly used as a means to consolidate metallic particles. Bulk materials of good mechanical properties are formed as a result of the process (Xia et al., 2007).

- **Glassy polymers**

(Weon et al., 2005) investigated the behavior of ECAP processed polymethylmethacrylate (PMMA) at 100°C with both routes A and C. The results have shown that the effect on the plastic and strength parameters (modulus of elasticity, strength/elongation to failure at tensile tests) on ECAP-processed PMMA samples is much less significant compared to the semicrystalline

polymers. (Yoshioka and Tsukamoto, 2009) investigated the ECAE of PMMA and PC by varying the processing temperature between 50 °C and up to Tg and the channel's angle between 90° and 150°. The study resulted in the successful ECAP processing of PC and PMMA samples within the specified range. As a general conclusion about glassy polymers, ECAP has proven to enhance the effects of crack and impact resistance of those materials while other characteristics would require additional investigations.

While this chapter mostly consisted of introducing polyethylene and equal channel angular processing, the following chapters of the thesis will focus on:

- A literature review about the work done on polymers and ECAP in addition to defining the objectives of the current work.
- A presentation of the designed experimental setups along with a discussion of the experimental results.
- A discussion of the shortcomings and some recommendations for future improvement.

Chapter 2
Literature Review

Polymers have an essential role in everyday life due to their wide range of applications including in electronics, aerospace, biomedical and automotive fields. Polymers are macromolecules that are either natural or synthetic, having distinctive physical and mechanical properties. Polymers are starting to replace metals in many applications due to their lower cost and weight. Three different types of polymers exist: elastomers, thermoplastics and thermosets. Elastomers are rubber-like materials that are highly elastic. The thermoplastics do not contain cross-bonds allowing them to be easily shaped using mold and are softened when heated while the thermosets start cross-linking when heated to become harder and infusible materials (Ayoub et al., 2011a; Hachour et al., 2014b; Makki et al., 2017). In this work, the main focus was on studying thermoplastics. Two categories of thermoplastics exist: amorphous and semi-crystalline. Amorphous thermoplastics consist of randomly oriented and entangled chains while the semi-crystalline thermoplastics are composed of regions of highly ordered and aligned chains in addition to the amorphous regions (Peacock, 2000).

More precisely, the effect of thermomechanical processing on different grades of semi-crystalline polyethylene will be studied. Polyethylene (PE) is one of the most commonly used semi-crystalline polymers due to its wide range of attainable mechanical properties. PE is used in different industrial applications among which are bottles, chemical storage tanks, food storage containers, toys, etc. (Peacock, 2000). Polyethylene is known for its semi-crystalline microstructure characterized by an ordered region called crystallites as well a region with

randomly dispersed chains knowns as the amorphous region. The mechanical behavior of polyethylene is highly time-dependent and non-linear. Polyethylene is also known for its ability to attain large strains.

The mechanical properties of semi-crystalline polymers depend on many factors such as the proportion of both phases, the size, orientation and shape of the crystalline lamellas. Other factors also affect the mechanical behavior such as the strain rate, the loading path and the temperature. It has been found that the temperature has a significant effect on the mechanical behavior of semi-crystalline polymers affecting the yield stress, strain hardening and initial Young's modulus which decrease as the temperature increases (Brooks et al., 1998; Pampillo and Davis, 1972b). The strain rate has also been found to have a significant effect on the yield stress, the plastic flow and the strain hardening (Ayoub et al., 2011a; Richeton et al., 2006). Semi-crystalline polymers are characterized by a highly anisotropic behavior that depends on the loading direction (Hachour et al., 2014b).

The high range of variability in the crystal content of PE, which could be between a few percent and up to around 90%, covers a wide range of mechanical properties of the material (H. Abdul-Hameed et al., 2014; Hemin Abdul-Hameed et al., 2014; Ayoub et al., 2011a; Peacock, 2000). At low crystallinity, PE has a quasi-elastomeric behavior and behaves more like a thermoplastic as the crystal content increases (Ayoub et al., 2011a). The deformation process of semi-crystalline polymers is dictated by the deformation of both the amorphous and the crystalline phases which are interconnected through covalent bonds (Bartczak and Galeski, 2010b). The amorphous phase of a semi-crystalline polymer consists of entangled chains that are randomly distributed and assumed to be isotropic. The deformation of a semi-crystalline polymer, prior to yield, begins with the unfolding and the stretching of the entangled chains in the amorphous region

where the weak bonds between them would break-up. This is followed by the rotation of the chains in the direction of the maximum principal stretch. During the plastic deformation of the semi-crystalline polymers, crystalline block segments are formed through the separation of the crystalline lamellae, followed by a reorientation of the crystalline segments and the amorphous linking in the direction of the maximum principal stretch. A significant strain hardening occurs until the chains reach failure (Elmeguenni et al., 2013).

The deformation mechanism of semi-crystalline polymers was investigated by several researchers (Bartczak, 2005; Bartczak and Galeski, 2010b, 2010a; Boulahia et al., 2009; Kazmierczak et al., 2005; Patlazhan and Remond, 2012; Rozanski and Galeski, 2013; Seguela et al., 1998a, 1998b). Different types of models have been developed to describe the mechanical behaviors of polymers. Two main modelling approaches are commonly adopted in developing constitutive models for polymers: the phenomenological and physical-based approached. In a phenomenological model, the empirical observations are related to the mathematical expressions that are consistent with the theories of thermodynamics. Different phenomenological models that describe the mechanical behavior of semi crystalline polymers have been developed (Bardenhagen et al., 1997; Ben Hadj Hamouda et al., 2007; Colak, 2005; Drozdov, 2009; Dusunceli and Colak, 2008; Ghorbel, 2008; Haward and Thackray, 1968; Khan and Zhang, 2001; Regrain et al., 2009; Zaïri et al., 2005a, 2005b, 2008). Other models based on physical-based modelling approach have been developed (Adams et al., 2000; Ahzi et al., 2003; Ames et al., 2009; Anand et al., 2009; Anand and Gurtin, 2003; Arruda et al., 1995; Ayoub et al., 2010; Belbachir et al., 2010; Boyce et al., 1988; Buckley and Jones, 1995; Dupaix and Krishnan, 2006; Makradi et al., 2005; Richeton et al., 2007; Tervoort et al., 1997; Wu and van der Giessen, 1995; Zaïri et al., 2011, 2010). This approach is composed of two main components: the first one is a purely based physical model

while the second one is partly physically-based coupled with a phenomenological model. (Ayoub et al., 2011b) developed a hyperelastic-viscoplastic model describing the mechanical behavior of polyethylene at different crystallinity rates. The model is composed of crystalline and amorphous resistances coupled with an eight chain model (Arruda and Boyce, 1993).

Equal Channel Angular Processing (ECAP or ECAE) is a severe plastic deformation technique that dates back to the early 70s and was developed by Segal. A simple shear is imposed on a sample by pushing it though an angular die of a constant cross-section (Vladimir M. Segal, 2017). As the sample is being extruded in its solid state, significant molecular reorientation takes place. Solid state extrusion is more effective in generating high degrees of molecular reorientation than those extruded in the molten state (Sue et al., 1999). Most of the previous studies that investigated ECAP were on metallic materials (V A Beloshenko et al., 2013; M Furukawa et al., 2001) while only a few studies addressed the mechanical behavior of polymeric materials (Campbell and Edward, 1999; Li et al., 2000; Sue and K.-Y.Li, 1998; Wang et al., 2006; Weon et al., 2005).

The first time ECAP was applied to polymers was by (Sue and K.-Y.Li, 1998). It was proven that the ECAP altered the morphology of linear low density polyethylene (LLDP). In case of polycarbonate (PC), (Sue et al., 1999) concluded that ECAP is the most effective when the extrusion is conducted at temperatures that are marginally under the glass transition temperature of PC. (Li et al., 2000) confirmed that the alteration of the mechanical properties of PC is possible through extruding using different processing routes and number of passes. (Xia et al., 2001a) studied the influence of the anisotropy on the impact strength of polycarbonate (PC) where the improvement of the impact resistance was found to be directly related to the changes of the molecular orientation caused by the ECAP. The molecular orientation and the

degree of crystallinity were identified to be important factors in the determination of the mechanical properties of the semicrystalline polyethyleneterephtalate (PET) processed through ECAP (Xia et al., 2001b). The fracture of the fiber-reinforced thermoplastics for ECAP-processed samples was studied by (Creasy and Kang, 2005). The fiber length was found to be controllable through having the process temperature to be below the melting point of polymer crystallites. (Weon et al., 2005) studied the impact of different ECAP routes on the different mechanical properties (tensile, fracture toughness, flexural) of polymethylmethacrylate (PMMA). (Wang et al., 2006) reported the lamellar formation and relaxation in simple sheared polyethylene terephthalate (PET) using the Small-Angle X-ray Scattering (SAXS) technique. (Aour et al., 2009; Bouaksa et al., 2014; Zaïri et al., 2008) investigated the effects of the geometrical and processing parameters of ECAP-processed polymers. (Aour and Mitsak, 2016) proved that ECAP is an effective process to alter the mechanical properties of polymers by inducing an anisotropy in the extruded material (Xia et al., 2001a). The ECAP technique is very versatile and can be easily added to be part of the processing of polymers (Sue et al., 1999).

While the fore mentioned studies focused on the modelling of Equal Channel Angular Processing or the investigation of the mechanical behavior of a certain type of polymers, none investigated the effect of ECAP on the mechanical behavior of different crystallinities of polyethylene. This goal would be achieved through the following steps:

- Designing the appropriate experimental setups to conduct the tests.
- Conducting the extrusion of the LDPE and HDPE samples at two main extrusion velocities (4.5 and 45mm/min) and four back-pressures (0, 375, 745 and 1120N) using a full factorial design.

- Characterizing the mechanical properties of the processed samples through tensile tests conducted at two strain rates: 2.58mm/min and 25.8mm/min.

Chapter 3
Experimental Setups and Results

3.1. Material

LDPE, HDPE and UHMWPE billets were purchased from Thyssenkrup Engineered Plastics with crystallinity degrees ranging between 38% and 76%. The billet samples were cut into 12.7x12.7x101.6 mm^3 in order to fit the dies for ECAP processing.

3.2. ECAP Billet Setup

The geometrical parameters of the ECAP die, namely the two angles $\emptyset$ and Ψ, determine the plastic shear strain applied to the sample as it is pushed through the die. The theoretical expression of the plastic shear strain is given by (Iwahashi et al., 1996):

$$\gamma = 2\cot\left(\frac{\phi}{2}+\frac{\Psi}{2}\right)+\Psi\,\mathrm{cosec}\left(\frac{\phi}{2}+\frac{\Psi}{2}\right) \qquad (2.1)$$

Homogeneous shear deformation is assumed in the processed sample. The die geometry parameters were adopted from the optimization study conducted by (Aour et al., 2008): a channel angle $\Phi = 90^{o}$, a corner angle $\Psi = 10^{o}$ and an inner radius $r = 2mm$ shown in Figure 3.1. The ECAP setup was mounted on the Intron 4469 ® UTM machine. The die was made of 304 stainless steel and composed of two parts clamped into each other as shown in Figure 3.2. The extrusion velocity was determined by the ram of the Instron 4469 ® and the back pressure was applied

through an HH Barnum ® double-acting single rod air cylinder connected to a controlled-pressure air supply. The assembly of the setup is shown in Figure 3.3.

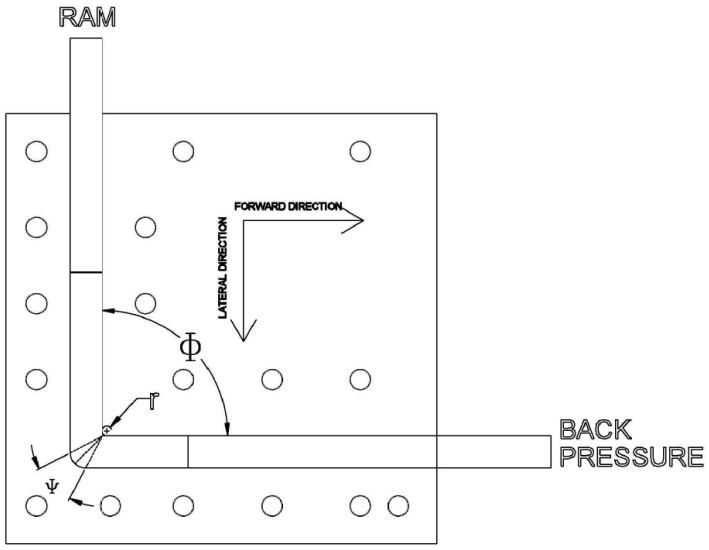

Figure 3.1: A schematic of the ECAP setup displaying the die's geometric angles.

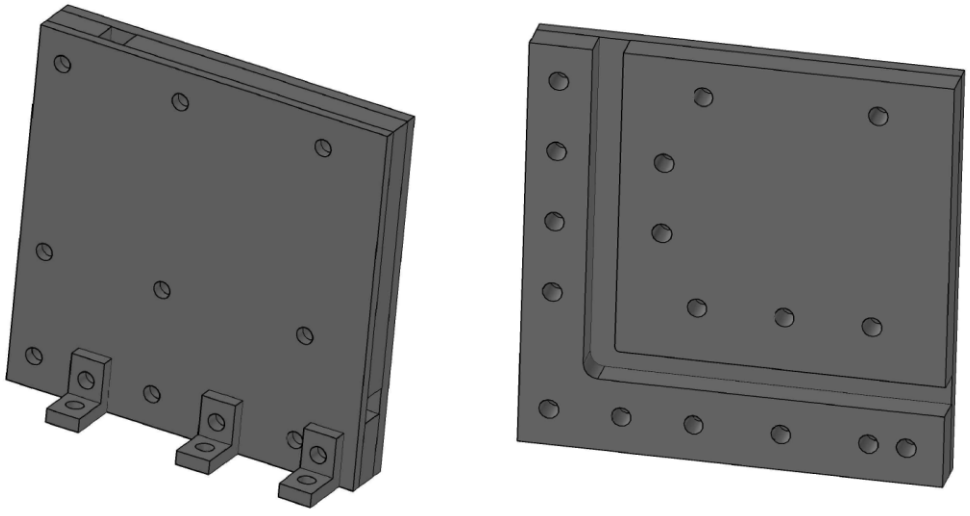

Figure 3.2: Three-dimensional drawings of the designed billet ECAP setup.

Figure 3.3: ECAP apparatus along with the back-pressure pneumatic cylinder system.

Figure 3.4 and Figure 3.5 show the detailed drawings of the manufactured adapters that are attached to the pneumatic cylinder and the UTM ram respectively. The drawings in Figure 3.6 and Figure 3.7 represent the attachment bars that are mounted on the other end of the adapters (Figure 3.3, Figure 3.4). A height adjustment plate shown in Figure 3.8 was designed to account for the height difference between the billet die and the pneumatic cylinder. Finally, the complete setup was fixated on a base plate (Figure 3.9) that was mounted on the UTM machine.

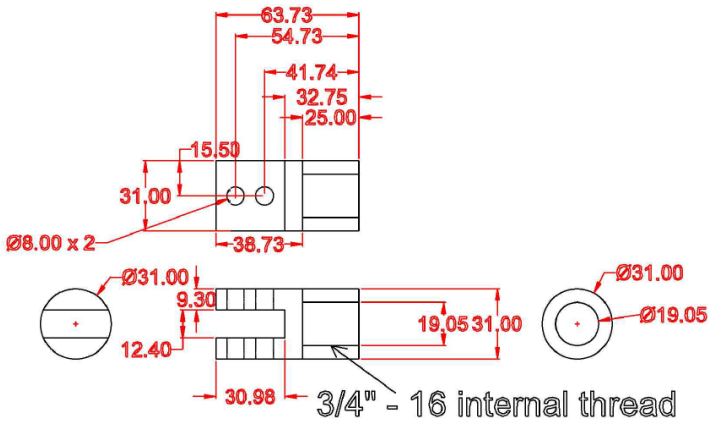

Figure 3.4: Adapter designed for the back-pressure pneumatic cylinder.

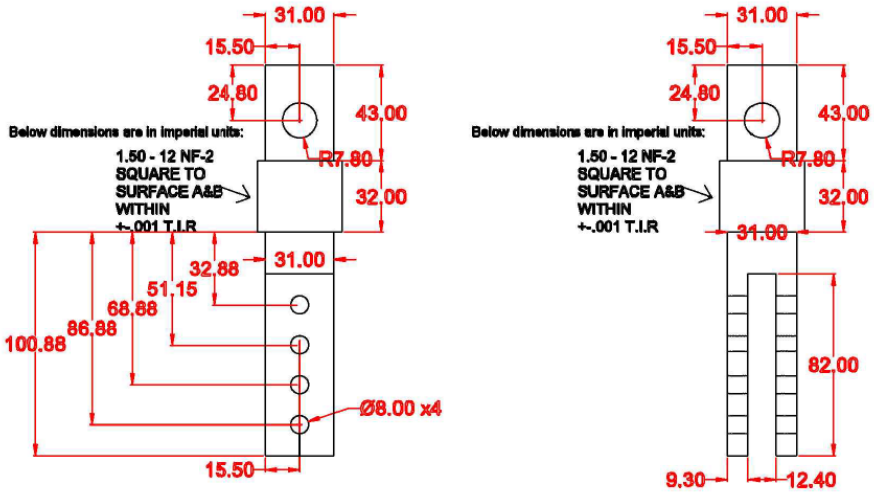

Figure 3.5: Adapter designed for the ram of the UTM tensile machine.

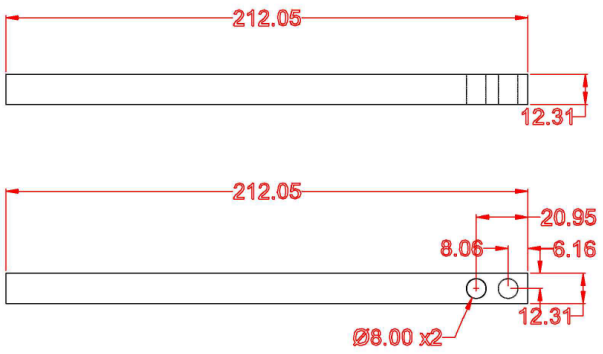

Figure 3.6: Attachment to the pneumatic cylinder.

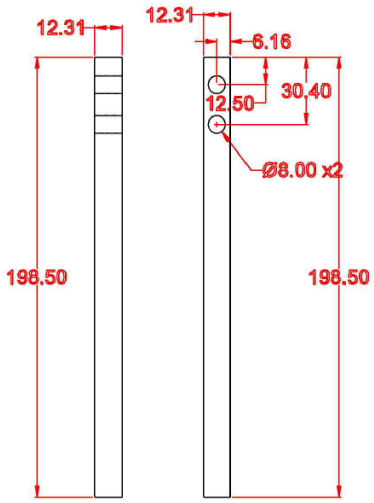

Figure 3.7: Attachment to the UTM ram.

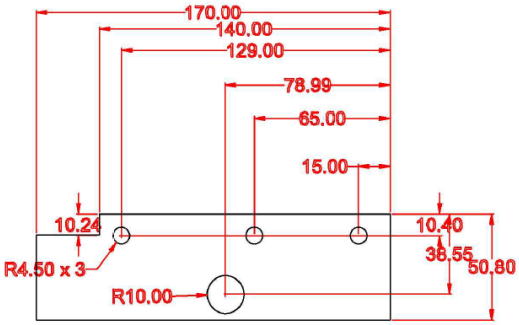

Figure 3.8: Height adjustment plate.

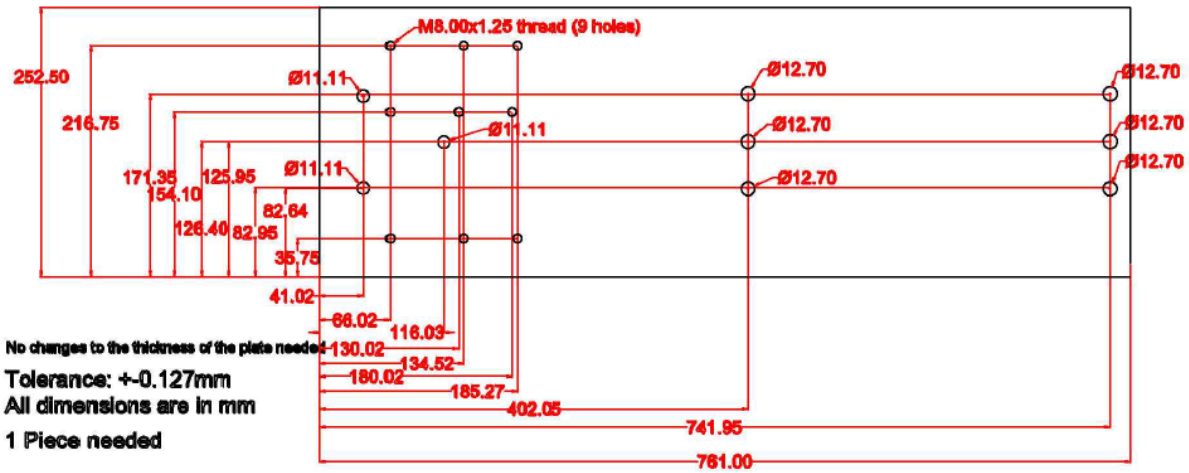

Figure 3.9: Assembly base plate.

3.3. ECAP Experiments

ECAP experiments were conducted at room temperature (about 23°C), under constant ram speeds of 4.5 and 45mm/min and a back-pressure ranging from 0N to 1120N. A full-factorial experimental design was adopted along with an additional test that was performed at an extrusion velocity of 0.45mm/min and a back-pressure of 0N for the three materials. Before inserting each of the as-received samples into the die, the samples were lubricated with an inert grease lubricant obtained from McMaster®. The load-displacement data were recorded for each extrusion. The test matrix of the conducted experiments is shown in Table 3.1.

Table 3.1: Test Matrix of the ECAP experiments representing the number of samples tested at each condition.

		Material								
		LDPE			HDPE			UHMW		
		Extrusion Velocity (mm/min)			Extrusion Velocity (mm/min)			Extrusion Velocity (mm/min)		
Back-Pressure (N)		0.45	4.5	45	0.45	4.5	45	0.45	4.5	45
	0	2	2	2	2	2	2	2	2	2
	375		2	2		2	2		2	2
	745		2	2		2	2		2	2
	1120		2	2		2	2		2	2

3.4. Tensile Setup

The tensile tests were conducted on the Instron testing machine using a 1kN load cell at room temperature under different cross-head speeds ranging from 2.58mm/min up to 258mm/min, i.e. a nominal strain rate of $10^{-3}s^{-1}$ to $10^{-1}s^{-1}$, using a specimen gage length of 43mm shown in Figure 3.10.

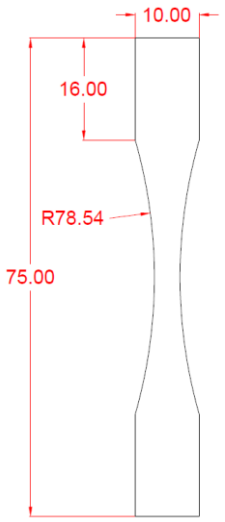

Figure 3.10: Two-dimensional drawing of the tensile testing specimen.

3.5. Tensile Tests

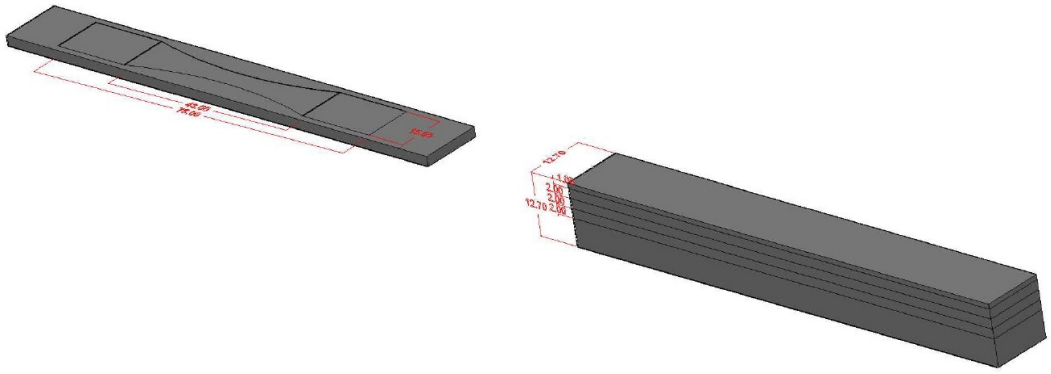

Figure 3.11: Illustration of the extraction of the tensile testing specimen.

After the ECAP, tensile specimens were machined from the ECAP material having the tensile axis aligned with the forward direction of the extrusion. Multiple layers were extracted from the processed plate and were cut into dog bone specimen as shown in Figure 3.11. The layers were cut using a PICO-155P Precision Cutter. There has been some difficulty in extracting a good quality top layer and in some cases a middle layer as well due to the curvature of the samples and the vibration of the blades. Tensile specimens were also machined from the as-received material to test the original properties of the material. Table 3.2 shows the different tensile tests performed for the tested ECAP conditions under two strain rates.

Table 3.2: Test matrix of the tensile tests representing the number of tests conducted at each condition.

Material	Extrusion Velocity (mm/min)	Back-Pressure (N)	Strain Rate (mm/min)	
			2.58	25.8
LDPE	0.45	0	1	1
	4.5	0	1	1
	4.5	375	1	1
	4.5	745	1	1
	4.5	1120	1	1
	45	0	1	1
	45	375	1	1
	45	745	1	1
	45	1120	1	1

Material	Extrusion Velocity (mm/min)	Back-Pressure (N)	Strain Rate (mm/min)	
			2.58	25.8
HDPE	0.45	0	1	1
	4.5	0	1	1
	4.5	375	1	1
	4.5	745	1	1
	4.5	1120	1	1
	45	0	1	1
	45	375	1	1
	45	745	1	1
	45	1120	1	1

3.6. ECAP Parameters Optimization

(i). In order to easily navigate through the plots of the ECAP extrusion results in sections 3.6, 3.7 and 3.8 the following notations are used:

(a) The experimental results of the specimens processed under the same back-pressure are presented using markers of the same shape (a circle represents a back-pressure of zero, a triangle represents a back-pressure of 375N, a square represents a back-pressure of 745N and a lozenge represents a back-pressure of 1120N).

(b) The experimental results of the specimens processed under an extrusion velocity of 4.5mm/min are presented with filled shapes markers while unfilled shapes markers are used to represent an extrusion velocity of 45mm/min and the extrusion velocity of 0.45mm/min is represented with a solid line without any markers.

(c) The as-received material on the graphs with the different ECAP conditions is represented with a dashed line.

(ii). The curves in section 2.4.1 and 2.5.1 of the strain rate sensitivity of the as-received material are represented as follows: the sample tested at a strain rate of 258mm/min is represented with

circle markers, a strain rate of 25.8mm/min is represented with square markers and a strain rate of 2.58mm/min is represented with triangular markers.

(iii). In the legends of the graphs, the term “ER” represents the extrusion rate or velocity followed by its value in mm/min, the term “BP” represents the back-pressure followed by its value in Newton and the term “SR” represents the strain rate followed by its value in mm/min.

3.6.1. High Density Polyethylene

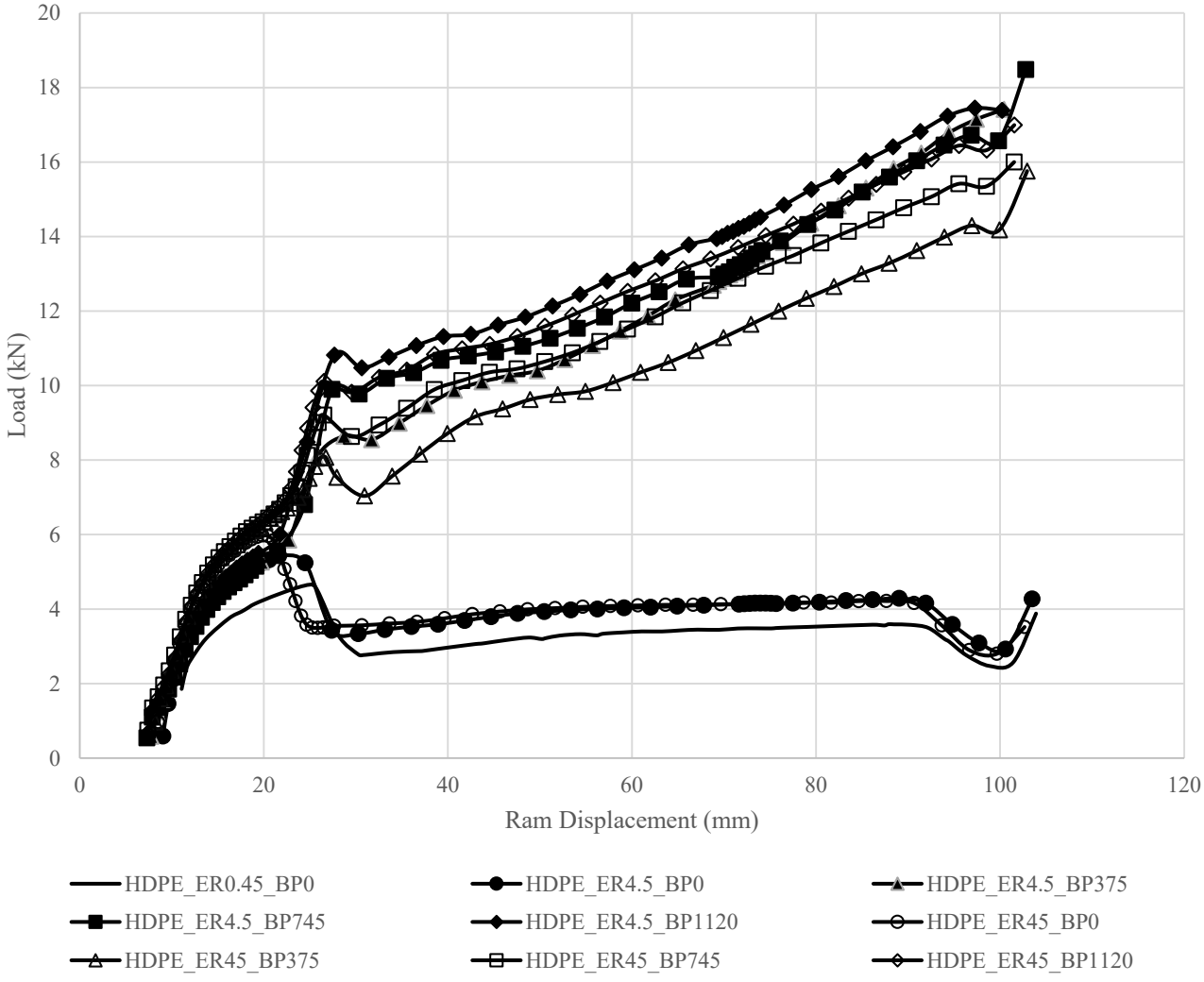

Figure 3.12: Force-Displacement curves during the ECAP pressing of HDPE samples with different parameters.

The effect of the extrusion velocity and the back-pressure on the load-ram displacement curves for the HDPE is shown in Figure 3.12. Varying the extrusion velocity has shown to have a lower effect on the load level required for the extrusion compared to the back-pressure. The application of a back-pressure ranging between 0N and 1120N increases the load level respectively regardless of the extrusion velocity. Figure 3.13 shows that the extruded HDPE samples completely filled the die with no reported ripples compared to (Hachour et al., 2014c), where the PP samples showed a rough upper surface.

3.6.1.1. Effects of the back-pressure

At a constant extrusion velocity, the load increases as the back pressure increases. At an extrusion speed of 4.5mm/min, varying the backpressure from 375N to 745N and up to 1120N, increases the yield load from 8.86kN to 10.01kN and 10.77kN respectively. It is worth noting that without any back-pressure the load level stabilizes as soon as the extrusion flow starts, while with the presence of back-pressure, the load keeps increasing until the end of the extrusion process due to the hardening induced by the back-pressure on the sample.

3.6.1.2. Effects of the extrusion velocity

The increase of the extrusion velocity resulted in the increase of both the load at yield and the slope of the force-ram displacement curve prior to yielding. The load at yielding of the HDPE samples increased from 4.68kN to 5.97kN as the extrusion velocity increased from 0.45mm/min to 45mm/min at a back-pressure of 0N. The increase of the extrusion velocity resulted in an increase of the load at yield from 8.05kN to 9.2kN at a back-pressure of 375N.

Figure 3.13: HDPE Samples: (a) Pressing Speed=45mm/min; Back Pressure= 0N, (b) Pressing Speed=4.5mm/min; Back Pressure= 1120N.

3.6.2. Low Density Polyethylene

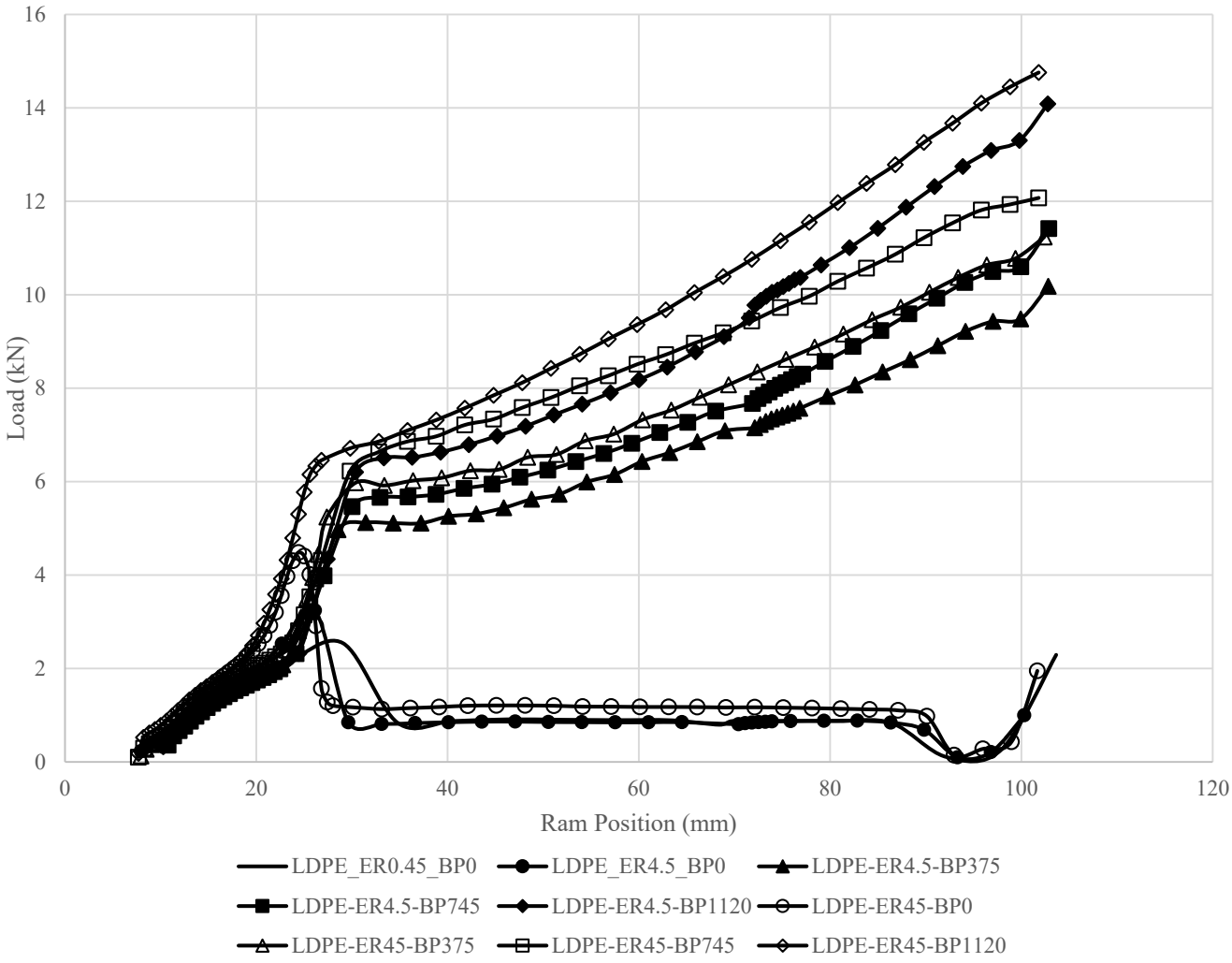

Figure 3.14: Force-Ram Displacement curves during the ECAP pressing of LDPE samples with different parameters.

The effect of the extrusion velocity and the back-pressure on the load-ram displacement curves for LDPE is shown in Figure 3.14 respectively. Varying the extrusion velocity has shown to have a lower effect on the load level required for the extrusion compared to the back-pressure. The application of a back-pressure ranging between 0N and 1120N increases the load level respectively regardless of the extrusion velocity. Figure 3.15 shows that the extruded HDPE

samples completely filled the die with no reported ripples compared to (Hachour et al., 2014c), where the PP samples showed a rough upper surface.

3.6.2.1. Effects of the back-pressure

At a constant extrusion velocity, the load increases as the back pressure increases. At an extrusion velocity of 4.5mm/min for the LDPE samples, varying the backpressure from 375N to 745N and up to 1120N, increases the yield load from 5.17kN to 5.63kN and 6.6kN respectively. It is worth noting that without any back-pressure for both HDPE and LDPE samples, the load level stabilizes as soon as the extrusion flow starts while with the presence of back-pressure, the load keeps increasing until the end of the extrusion process due to the hardening induced by the back-pressure on the sample.

3.6.2.2. Effects of the extrusion velocity

The increase of the extrusion velocity resulted in the increase of both the load at yield and the slope of the force-ram displacement curve prior to yielding. The load at yielding for the LDPE samples increased from 3.08kN to 4.55kN as the extrusion velocity increased from 0.45mm/min to 45mm/min at a back-pressure of 0N. The increase of the extrusion velocity resulted in an increase of the load at yield from 5.46kN to 6.22kN at a back-pressure of 375N and from 5.66kN to 6.71kN at a back-pressure of 745N.

Figure 3.15: LDPE Sample: (a) Pressing Speed=45mm/min; Back Pressure= 0N,
(b) Pressing Speed=45mm/min; Back Pressure= 1120N.

3.6.3. Ultra-High Molecular Weight Polyethylene

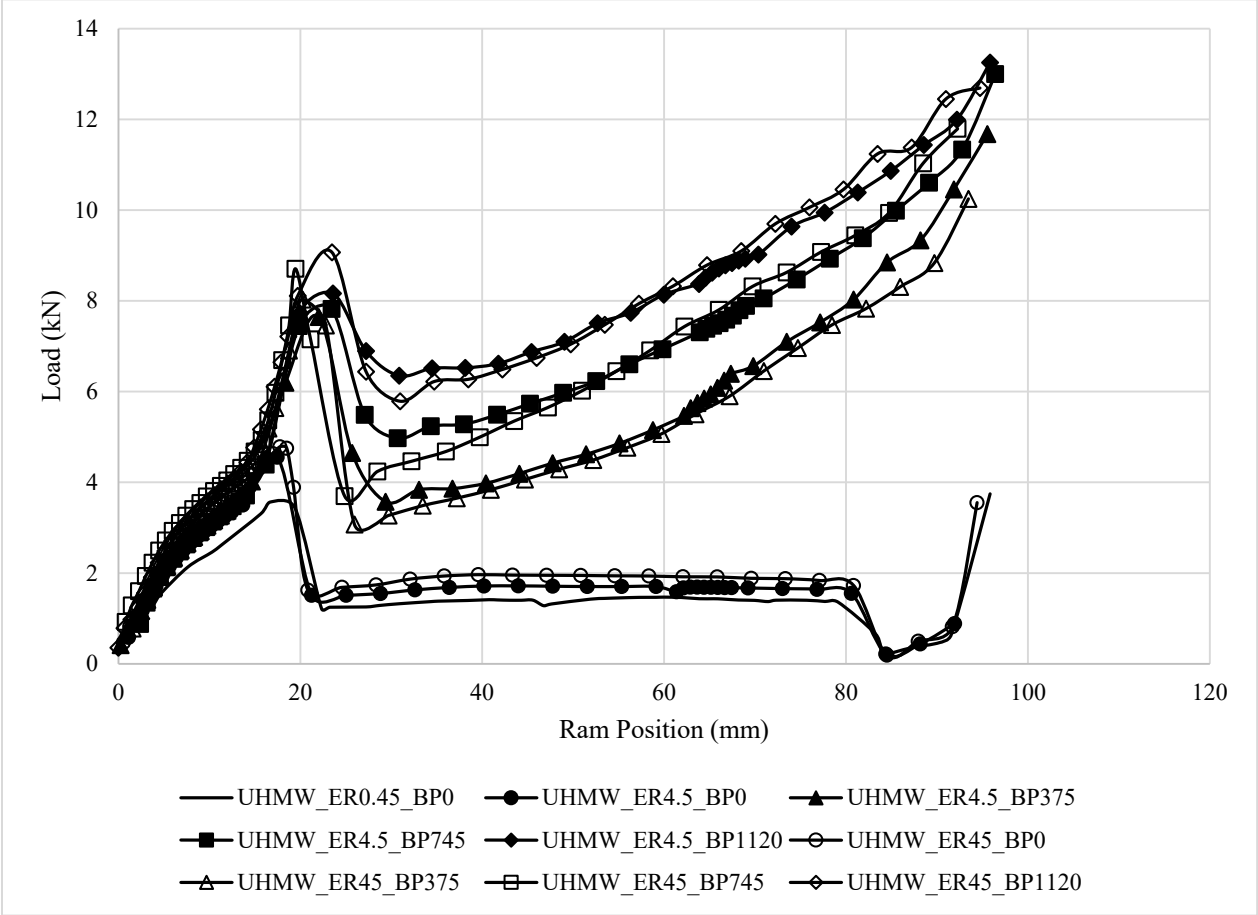

Figure 3.16: Force-Ram Displacement curves during the ECAP pressing of UHMWPE samples with different parameters.

The effect of the loading rate and the back-pressure on the load-ram displacement curves for the UHMWPE samples are shown in Figure 3.16. The increase of either the back-pressure from 0N to 1120N or the extrusion velocity from 4.5mm/min to 45mm/min results in the increase of the

load levels. Figure 3.17 shows that the extruded HDPE samples completely filled the die with no reported ripples compared to (Hachour et al., 2014c), where the PP samples showed a rough upper surface.

3.6.3.1. Effects of the back-pressure

At a constant extrusion velocity, the load increases as the back pressure increases. At an extrusion speed of 4.5mm/min, varying the backpressure from 375N to 745N and up to 1120N, increases the yield load from 7.78kN to 8.2kN and 8.3kN respectively. It is worth noting that without any back-pressure, the load level stabilizes as soon as the extrusion flow starts while with the presence of back-pressure, the load keeps increasing until the end of the extrusion process due to the hardening induced by the back-pressure on the sample.

3.6.3.2. Effects of the extrusion velocity

The increase of the extrusion velocity of the samples resulted in the increase of both the load at yield and the slope of the force-ram displacement curve prior to yielding. The load at yielding of the UHMWPE samples increased from 3.91kN to 4.81kN as the extrusion velocity increased from 0.45mm/min to 45mm/min at a back-pressure of 0N. The increase of the extrusion velocity resulted in an increase of the load at yield from 7.63kN to 8.3kN at a back-pressure of 375N and from 8.04kN to 8.96kN at a back-pressure of 745N.

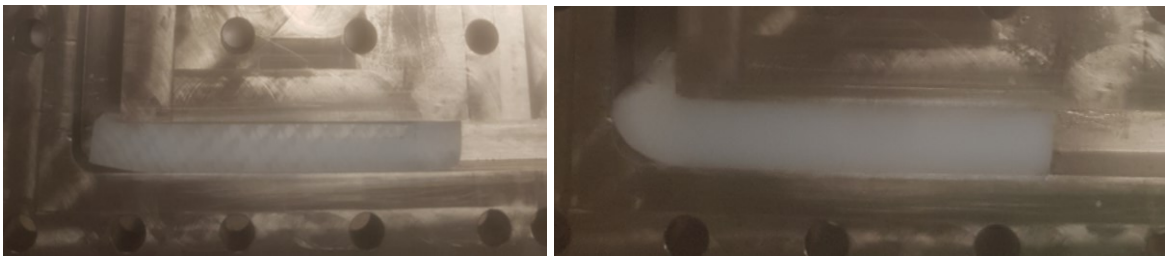

Figure 3.17: UHMWPE Sample: (a) Pressing Speed=45mm/min; Back Pressure= 0N, (b) Pressing Speed=4.5mm/min; Back Pressure= 1120N.

3.6.4. Effects of the degree of crystallinity

The extrusion process for HDPE required the highest extrusion load followed by UHMWPE and LDPE for a sample under the same experimental conditions. At the same extrusion velocity of 4.5mm/min, HDPE required 380% more load to be extruded than the LDPE that was extruded with a load of 0.85kN while UHMWPE required 357% more load than the LDPE. With the use of a back-pressure of 745N and an extrusion velocity of 45mm/min, the HDPE required a 77% higher than the LDPE that was extruded at a 6.81kN load while UHMWPE required 31.5% more load than LDPE.

3.7. Mechanical Characterization of HDPE

3.7.1. Characterization of the as-received material

Tensile tests have been conducted for the as-received HDPE specimens at three different nominal strain rates: 10^{-1}, 10^{-2} and $10^{-3}s^{-1}$ corresponding to 258, 25.8 and 2.58 mm/min respectively. The engineering stress-strain curves of the HDPE specimens are shown in Figure 3.18. As the strain rate increased, the total strain decreased and the yield strength increased.

The increase of the strain rate for the HDPE samples from 2.58mm/min to 258mm/min decreased the total strain to fracture 14% to 6.8%. The yield strength increased from 16.88MPa to 26.8MPa for the HDPE samples with the increase of the strain rate from 2.58mm/min to 258mm/min.

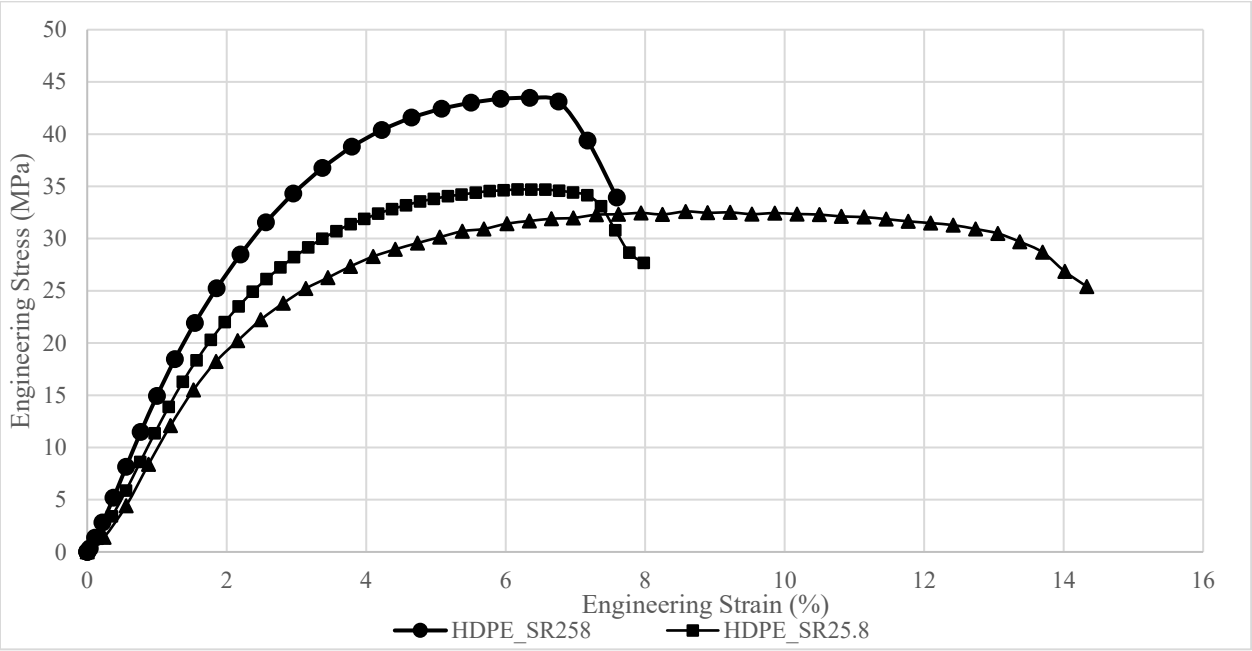

Figure 3.18: As-received virgin HDPE material tested at various strain rates.

3.7.2. Characterization of the ECAP samples

The results of the tensile tests are shown for each ECAP condition at two different strain rates 2.58mm/min and 25.8mm/min for both HDPE. All ECAP experiments have shown a lower yield strength compared to the as-received material. Figure 3.19 and Figure 3.20 show the HDPE ECAPed samples engineering stress – strain behavior at different strain rates 2.58mm/min and 25.8mm/min, respectively. In each plot, the behavior of the HDPE ECAPed specimens is compared to the as-received HDPE material. The engineering stress-strain curve begins with an

elastic region where the stress keeps increasing until yielding (which corresponds to the necking of the specimen) after which the stress increases at a lower rate until it starts decreasing.

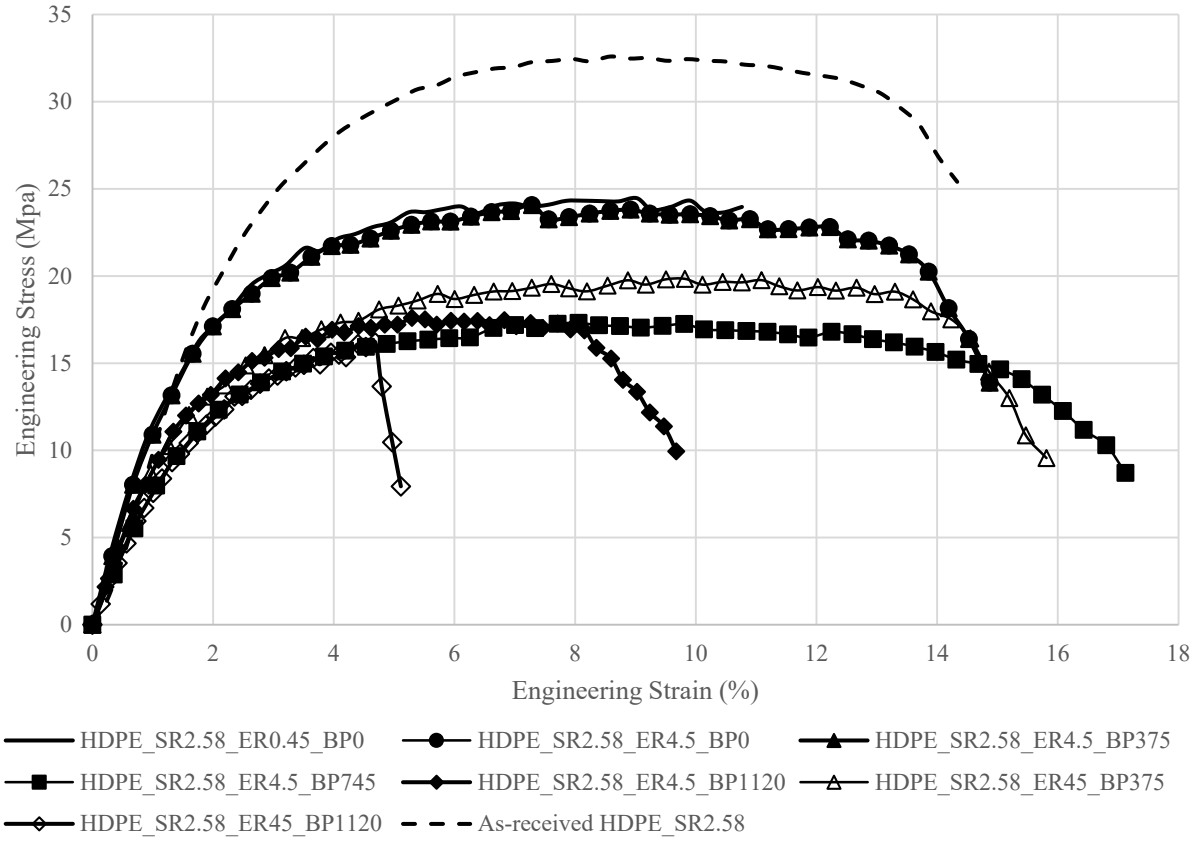

Figure 3.19: Force-Displacement curves of the ECAP-ed HDPE tensile specimen at a 0.001s-1 strain rate.

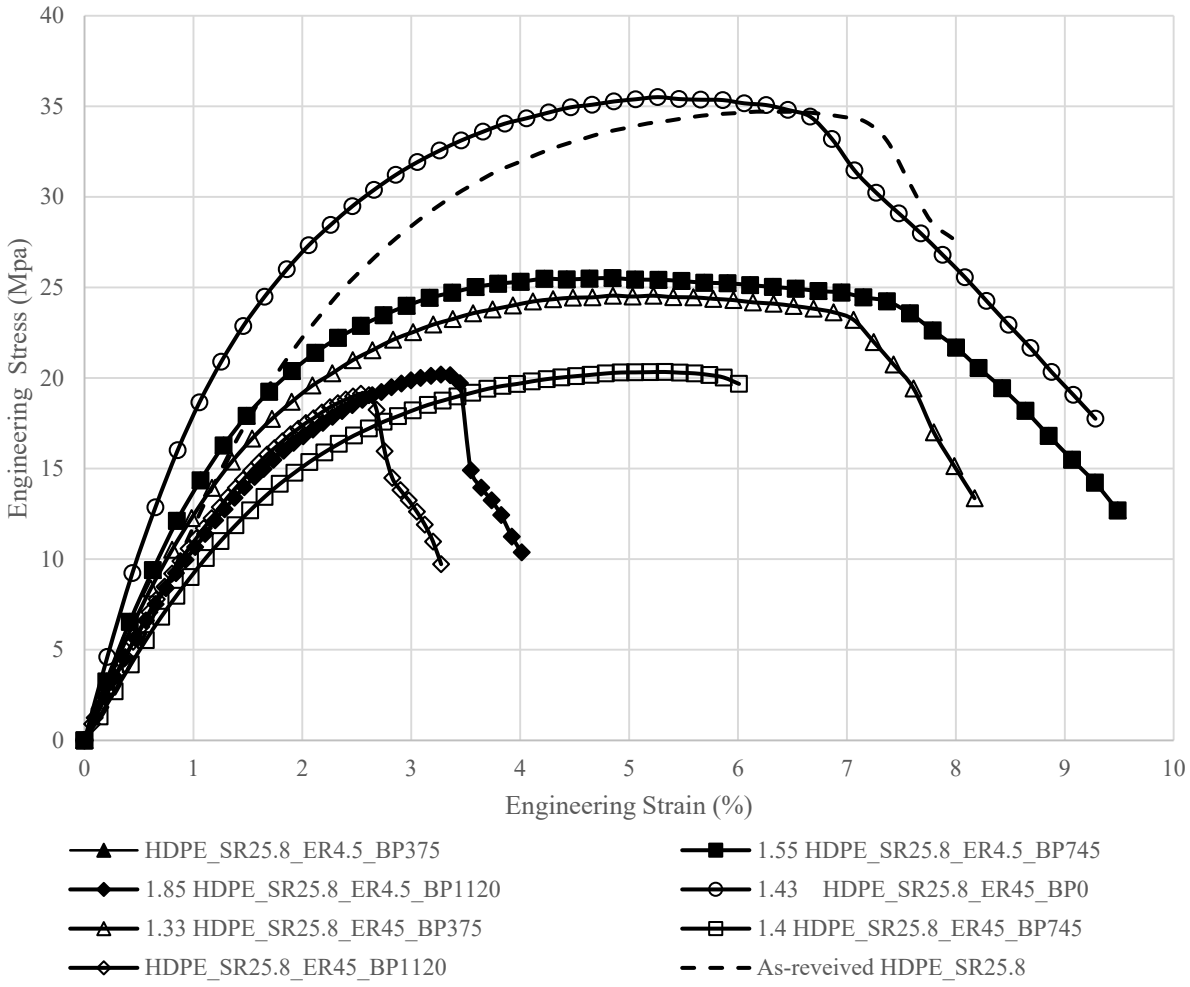

Figure 3.20: Force-Displacement curves of the ECAP-ed HDPE tensile specimen at a 0.01s-1 strain rate.

3.7.2.1. Effect of the back-pressure:

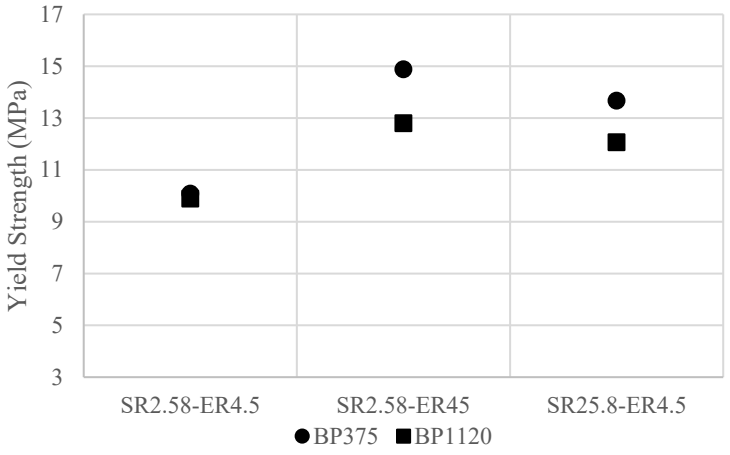

Figure 3.21: Evolution of the Yield Strength as a function of the back-pressure.

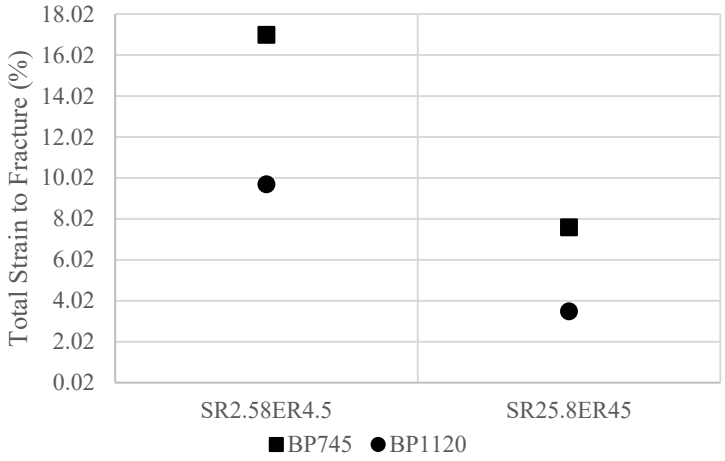

Figure 3.22: Evolution of the total strain to fracture as a function of the back-pressure.

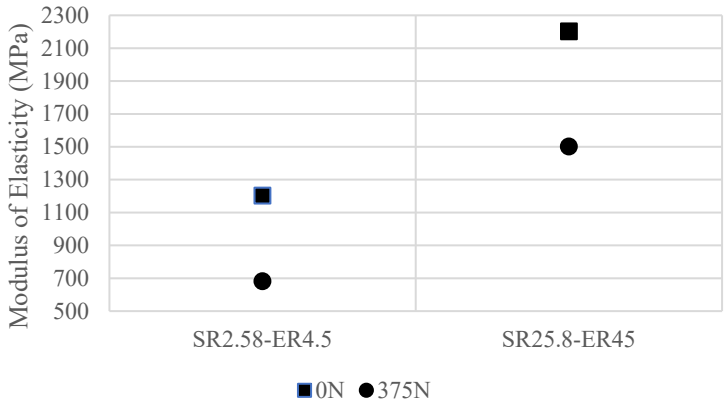

Figure 3.23: Evolution of the modulus of elasticity as a function of the back-pressure.

Applying a back-pressure to the extruded samples resulted in the decrease of the yield strength, the total strain to fracture and the modulus of elasticity for the HDPE specimens. The yield strength for the HDPE tensile samples tested at a strain rate of 2.58mm/min and extruded at a velocity of 4.5mm/min decreased from 10.08MPa to 9.89MPa as the back-pressure increased from 375N up to 1120N (Figure 3.21). The total strain to fracture also decreased from 14.8% to 7.8% with the increase of the back-pressure from 375N to 1120N (Figure 3.22). The modulus of elasticity decreased from 1202.1MPa to 681.84MPa as the back-pressure increased from 0N to 375N at a strain rate of 2.58mm/min and an extrusion velocity of 4.5mm/min (Figure 3.23).

3.7.2.2. Effect of the extrusion velocity

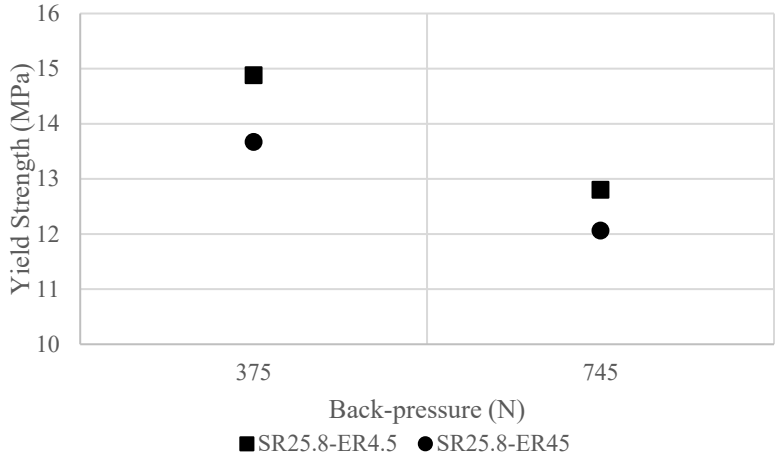

Figure 3.24: Evolution of the Yield Strength as a function of the extrusion rate.

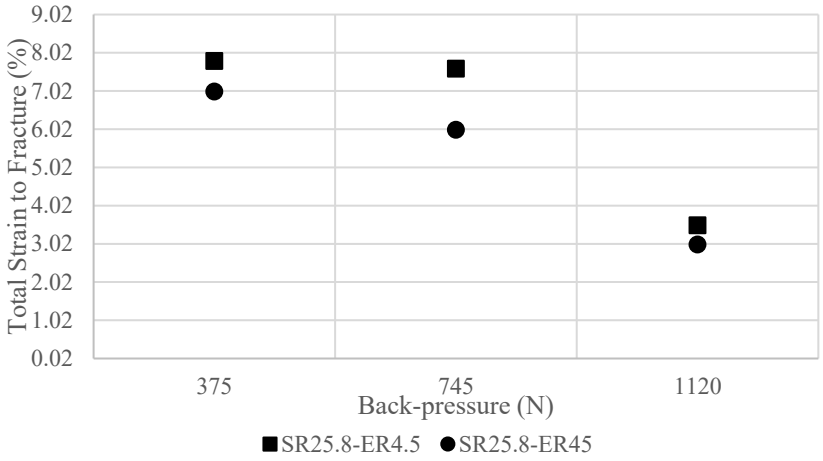

Figure 3.25: Evolution of the total strain to fracture as a function of the extrusion rate.

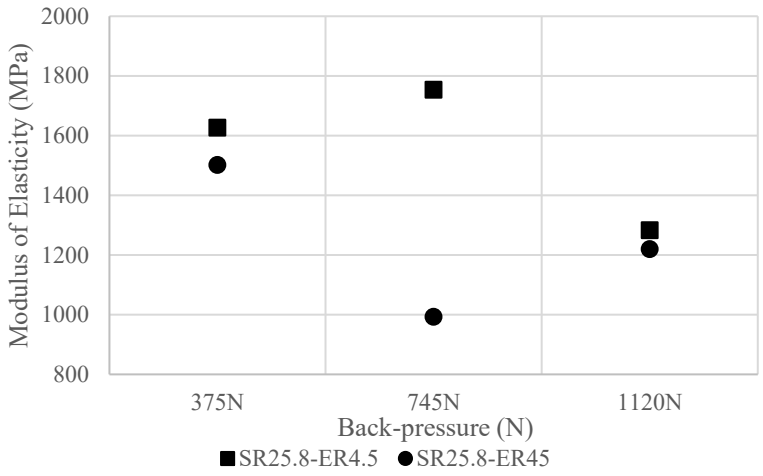

Figure 3.26: Evolution of the modulus of elasticity as a function of the extrusion rate.

For the HDPE samples, the increase of the extrusion velocity resulted in a decrease of the yield strength, the total strain to fracture and the modulus of elasticity.

The yield strength for HDPE samples tested at a 25.8mm/min strain rate and a back-pressure of 745N, the yield strength increased from 12.8MPa to 12.06MPa as the extrusion velocity increased from 4.5mm/min to 45mm/min. The total strain to fracture decreased from 7.6% to 6% as the extrusion velocity increased from 4.5mm/min to 45mm/min. The modulus of elasticity decreased from 1626.3MPa to 1501.6 with the increase of the extrusion velocity at a back-pressure of 375N and a strain rate of 25.8mm/min (Figure 3.26).

3.7.2.3. Effect of the strain rate

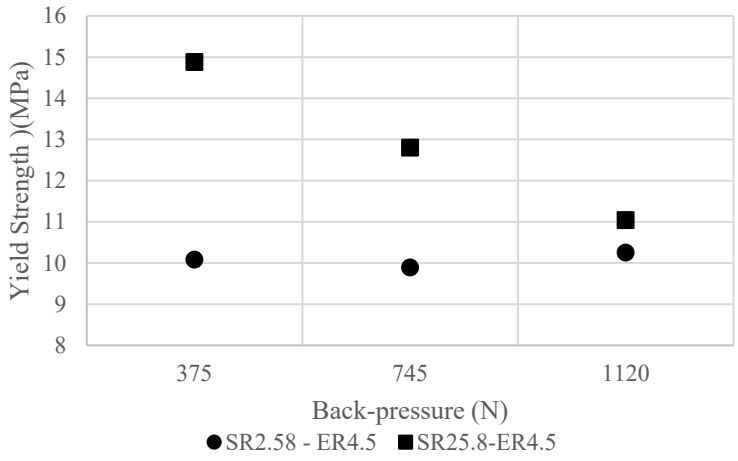

Figure 3.27: Evolution of the Yield Strength as a function of the strain rate.

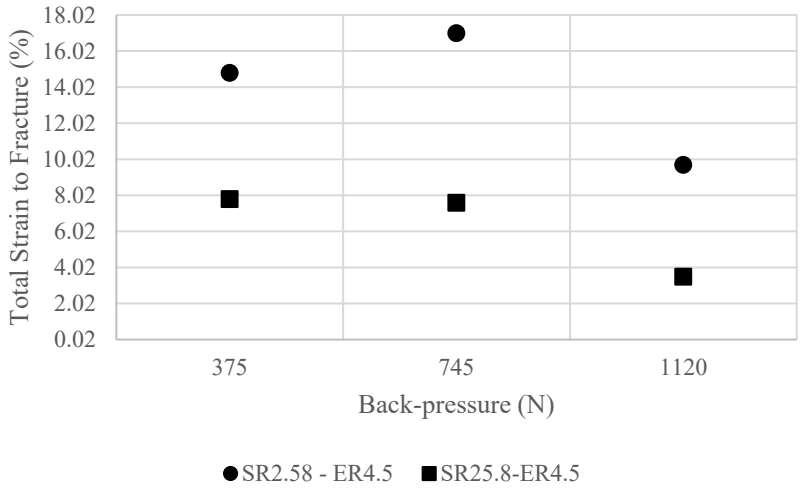

Figure 3.28: Evolution of the total strain to fracture as a function of the strain rate.

Increasing the strain rate of the tested HDPE tensile samples resulted in an increase in the yield strength and a decrease in the total strain to fracture. At an extrusion velocity of 4.5mm/min and a back-pressure of 375N, the yield strength increased from 10.08MPa to 14.88MPa as the strain rate increased from 2.58mm/min to 25.8mm/min. The total strain to fracture also decreased from 14.8% to 7.8% as the strain rate increased from 2.58mm/min to 25.8mm/min.

3.8. Mechanical Characterization of LDPE

3.8.1. Characterization of the as-received material

Tensile tests have been conducted for the as-received LDPE samples at three different nominal strain rates: 10^{-1}, 10^{-2} and $10^{-3}s^{-1}$ corresponding to 258, 25.8 and 2.58 mm/min respectively. The engineering stress-strain curves of the LDPE samples are shown in Figure 3.29. As the strain rate increased, the total strain to fracture decreased and the yield strength increased.

The increase of the strain rate for the LDPE samples from 2.58mm/min to 258mm/min decreased the total strain to fracture from 62% to 28.8% for the LDPE. The yield strength increased from 3.52MPa to 4.6MPa with the increase of the strain rate from 2.58mm/min to 258mm/min.

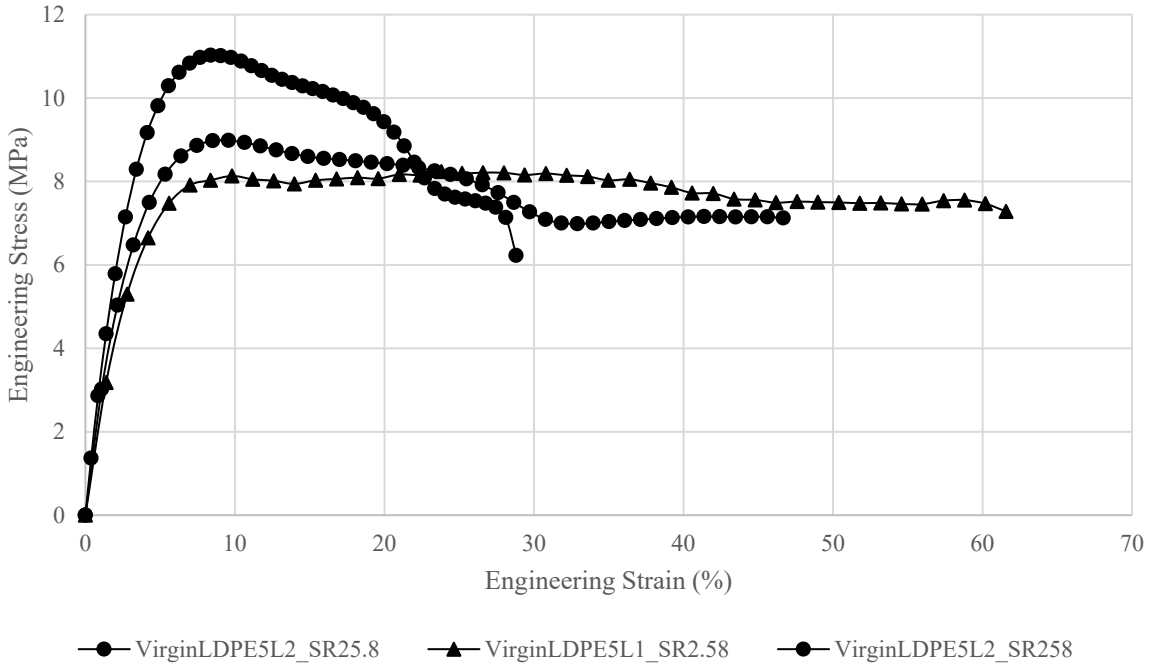

Figure 3.29: As-received virgin LDPE material tested at various strain rates.

3.8.2. Characterization of the ECAP samples

The results of the tensile tests are shown in each ECAP condition at two different strain rates 2.58mm/min and 25.8mm/min for LDPE. All ECAP experiments have shown a lower load level at yield compared to the as-received material.

Figure 3.28 show the different LDPE ECAP samples at different conditions compared to a virgin LDPE sample tested at a strain rate of 2.58mm/min and 25.8mm/min respectively. The engineering stress-strain curve begins with an elastic region where the stress keeps increasing until yielding (which corresponds to the necking of the sample) after which the stress stabilizes and slowly drops until failure.

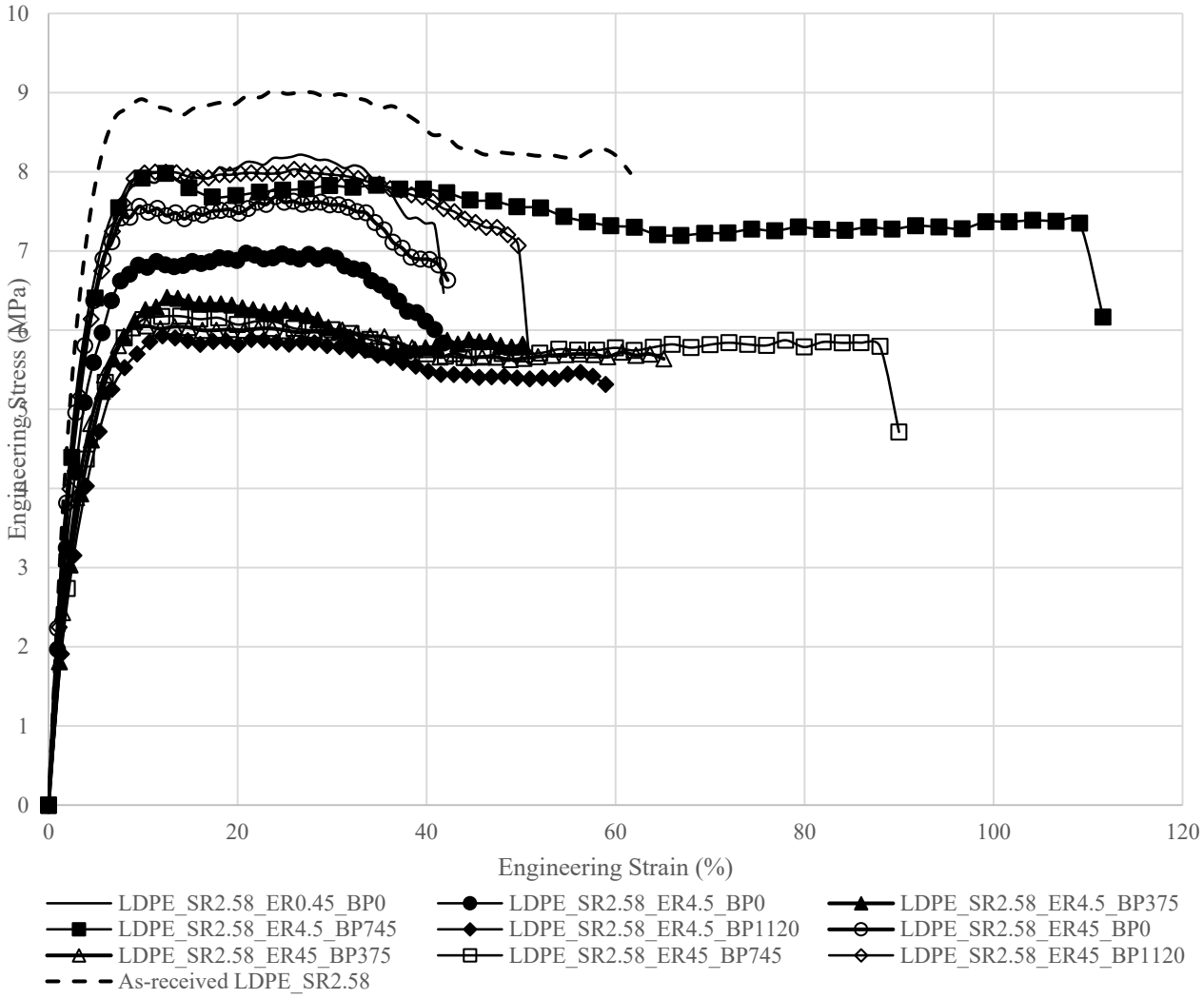

Figure 3.30: Force-Displacement curves of the ECAP-ed LDPE tensile specimen at a 0.001s-1 strain rate.

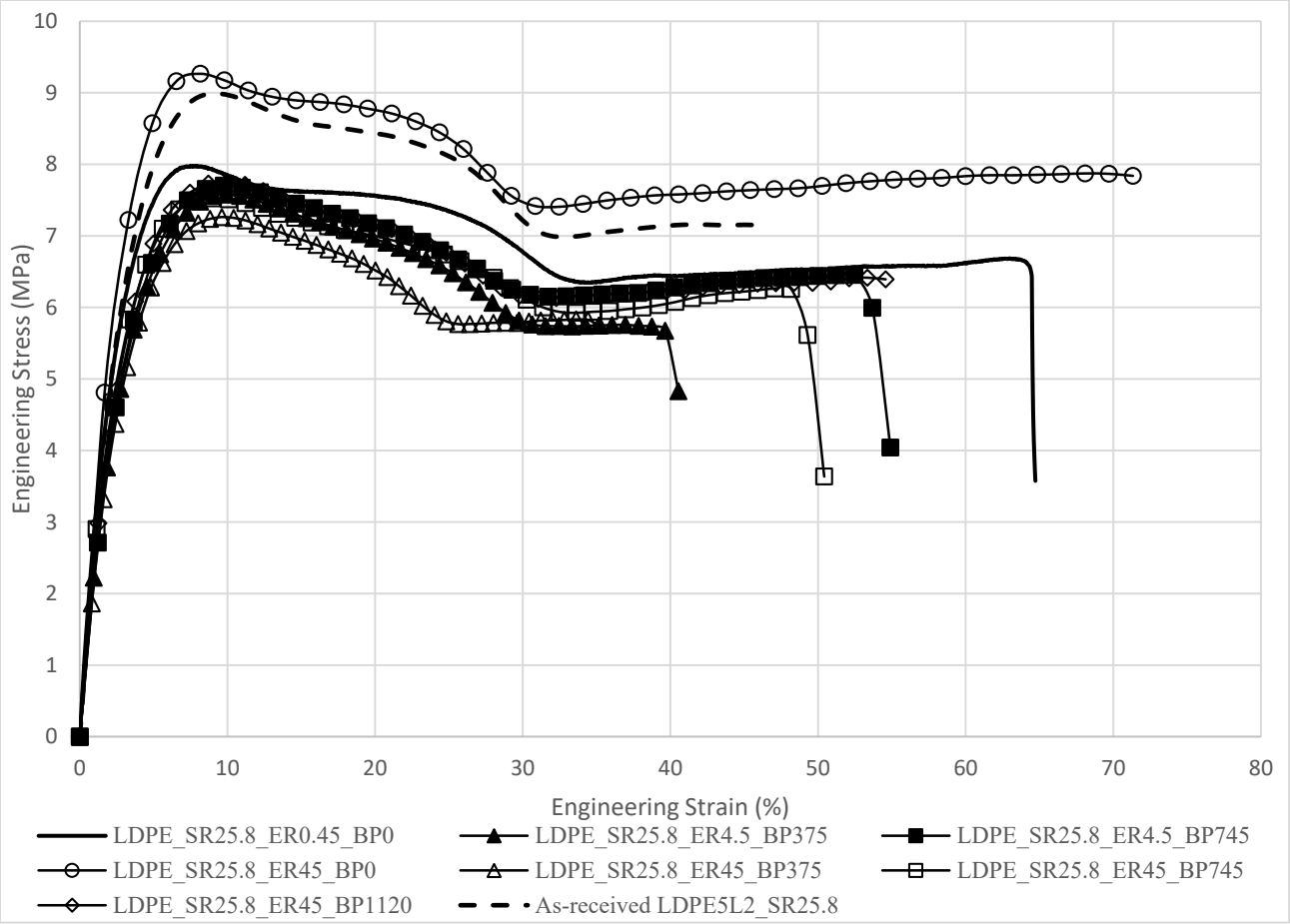

Figure 3.31: Force-Displacement curves of the ECAP-ed LDPE tensile specimen at a 0.01s-1 strain rate.

3.8.2.1. Effect of the back-pressure

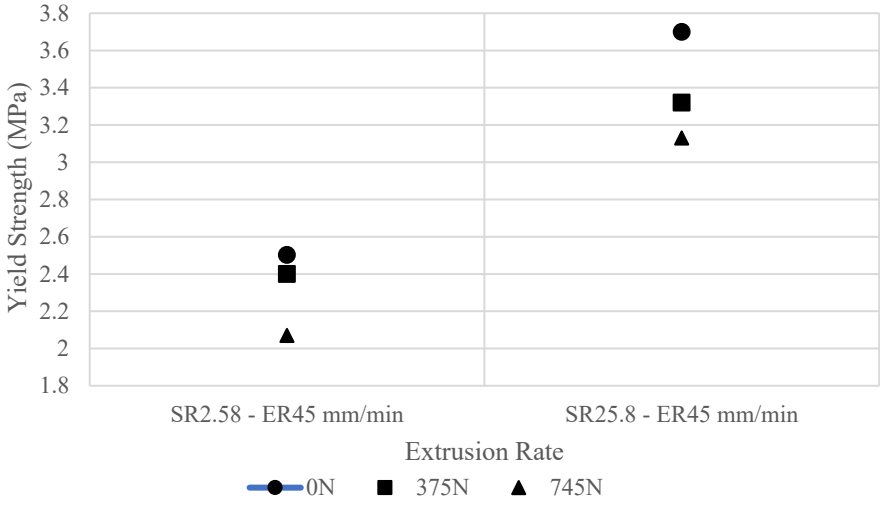

Figure 3.32: Evolution of the Yield Strength as a function of the back-pressure.

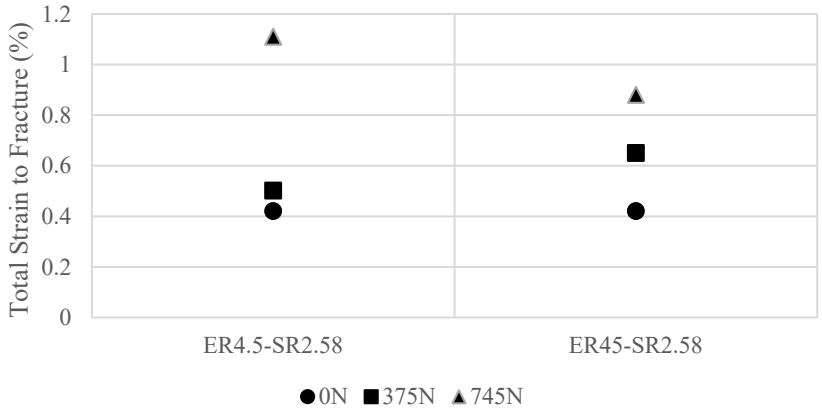

Figure 3.33: Evolution of the total strain to fracture as a function of the back-pressure.

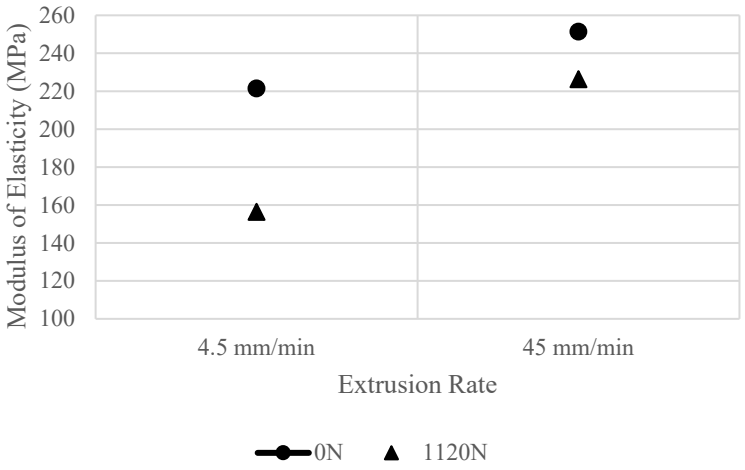

Figure 3.34: Evolution of the Modulus of Elasticity as a function of the back-pressure.

Applying a back-pressure to the extruded samples resulted in a general decrease of the yield strength and modulus of elasticity and an increase in the total strain to fracture for the LDPE samples (Figure 3.32, Figure 3.33 and Figure 3.34).

The LDPE tensile samples tested at a strain rate of 2.58mm/min and extruded at a velocity of 45mm/min, the yield strength decreased from 2.502MPa to 2.07MPa as the back-pressure increased from 0N to 1120N. The total strain to fracture increased from 42% to 88% with the increase of the back-pressure from 0N to 745N at an extrusion rate of 45mm/min and a strain rate of 2.58mm/min. The modulus of elasticity decreased from 221.42MPa to 156.43MPa as the back-pressure increased from 0N to 1120N at an extrusion velocity of 4.5mm/min and a strain rate of 2.58mm/min.

3.8.2.2. Effect of the extrusion velocity

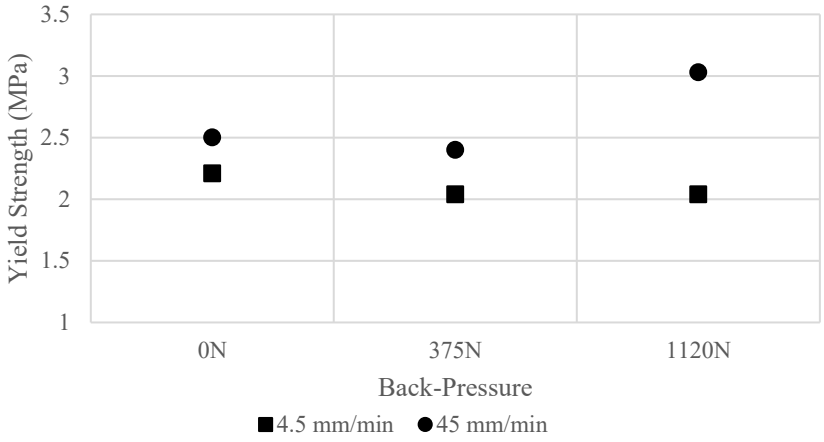

Figure 3.35: Evolution of the Yield Strength as a function of the extrusion velocity.

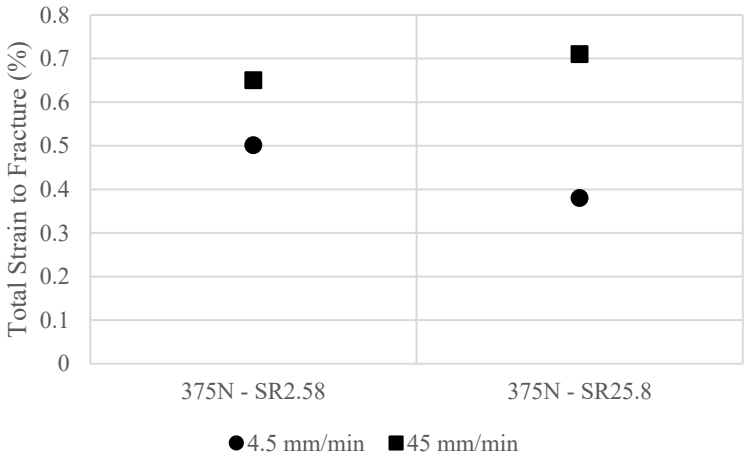

Figure 3.36: Evolution of the total strain to fracture as a function of the extrusion velocity.

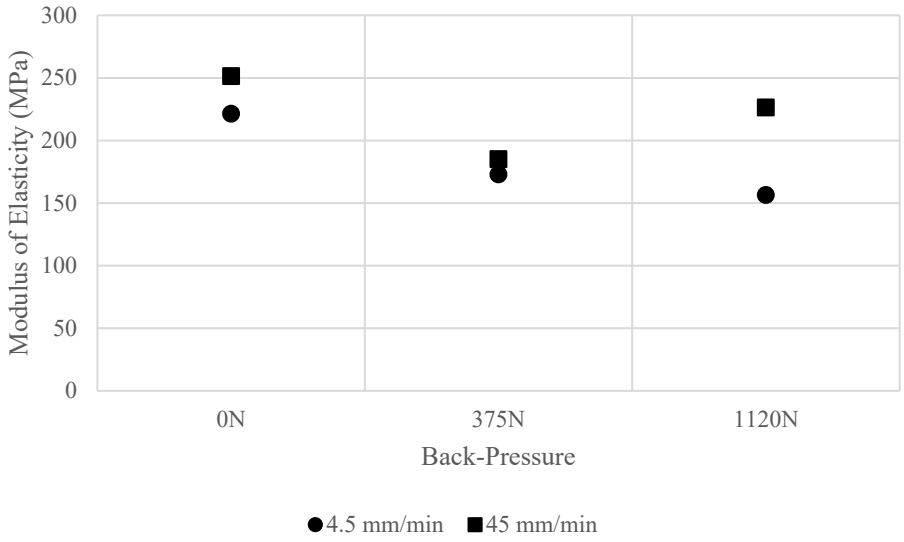

Figure 3.37: Evolution of the Modulus of Elasticity as a function of the extrusion velocity.

The extrusion velocity resulted in an increase of the yield strength, the total strain to fracture and the modulus of elasticity of the LDPE samples. The yield strength of the LDPE samples tested at a strain rate of 2.58mm/min and a back-pressure of 375N (Figure 3.35), the yield strength increased from 2.04MPa to 2.4MPa as the extrusion velocity increased from 4.5mm/min to 45mm/min. The total strain to fracture increased from 50.1% to 65% with the increase of the extrusion velocity at a back-pressure of 375N and a strain rate of 2.58mm/min (Figure 3.36). The modulus of elasticity increased from 221.42MPa to 251.35MPa as the extrusion rate increased at a constant back-pressure of 0N and a strain rate of 2.58mm/min (Figure 3.37).

3.8.2.3. Effect of the strain rate

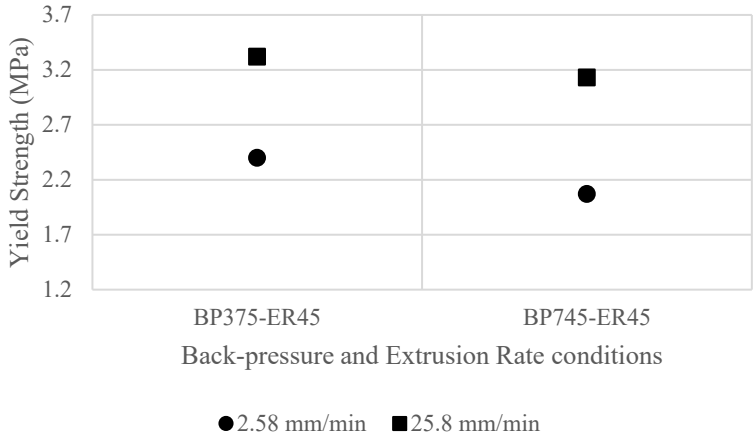

Figure 3.38: Evolution of the Yield Strength as a function of the strain rate.

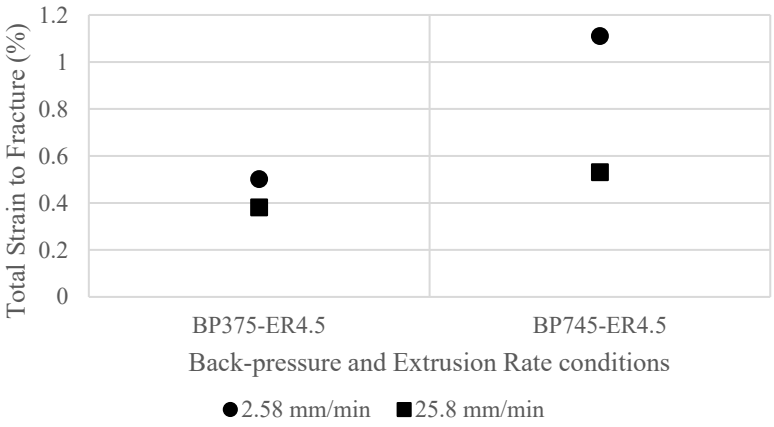

Figure 3.39: Evolution of the total strain to fracture as a function of the strain rate.

The increase of the strain rate resulted in an increase in the yield strength (Figure 3.38) but a decrease in the total strain to fracture (Figure 3.39). At a strain rate of 4.5mm/min and a back-pressure of 375N, the yield strength increased from 2.4MPa to 3.32MPa when the strain rate was increased from 2.58mm/min to 25.8mm/min. The total strain to fracture decreased from 50% to 38% under the same conditions.

3.9. Comparison of both crystallinities of polyethylene

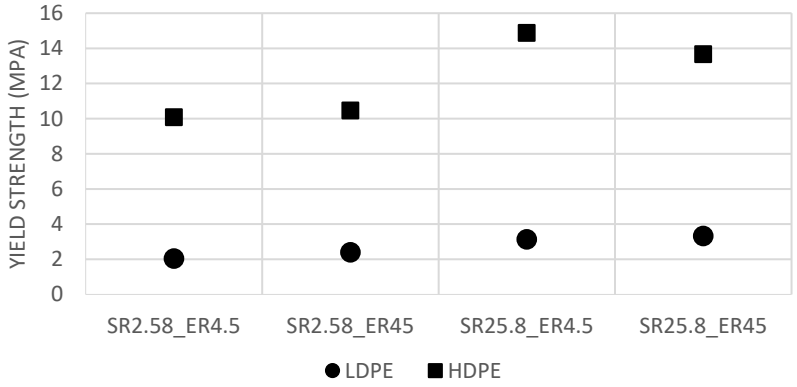

Figure 3.40: Evolution of the yield strength as a function of different crystallinities of polyethylene at a back-pressure of 375N.

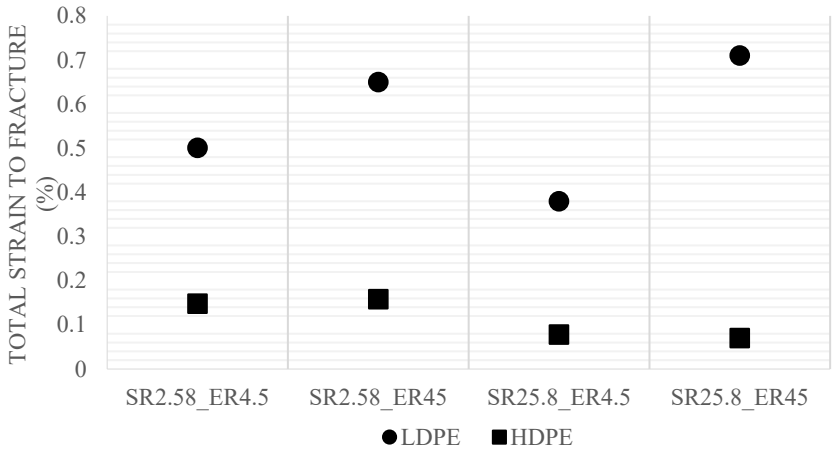

Figure 3.41: Evolution of the total strain to fracture as a function of different crystallinities of polyethylene at a back-pressure of 745N.

The higher crystallinity of polyethylene, the HDPE, exhibited a higher yield strength at the different tested conditions compared to the polyethylene with the lower crystallinity, LDPE as shown in Figure 3.40. For instance, the yield strength of HDPE was on average 350% higher than that of LDPE for the samples tested at a back-pressure of 375N.

As for the total strain to fracture, the lower crystallinity of polyethylene, the LDPE, exhibited a higher total strain to fracture at the different tested conditions compared to the polyethylene with the higher crystallinity, HDPE as shown in Figure 3.41. The total strain to fracture of LDPE was on average 393% higher than that of HDPE for the samples tested at a back-pressure of 745N.

Chapter 4
Recommendations, Suggestions for Improvement and Conclusions

4.1. ECAP Billet Setup

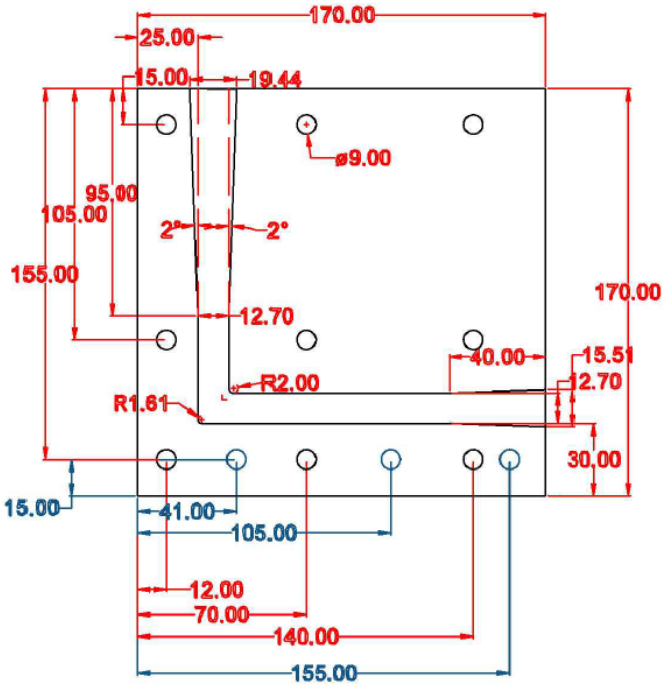

Figure 4.1: Suggested changes to the ECAP Billet die.

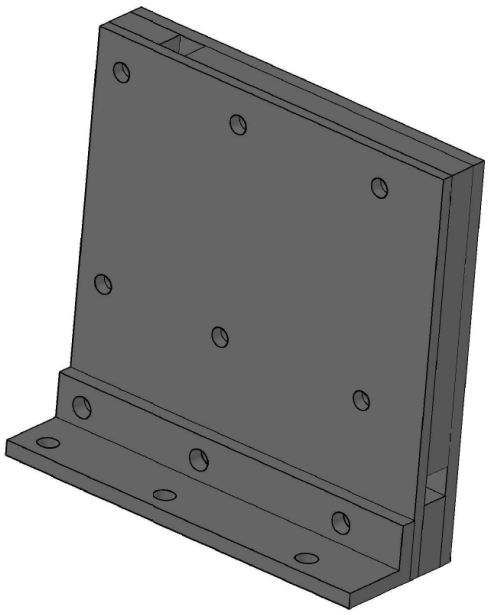

Figure 4.2: Suggested mounting setup for the die.

During the first batch of experiments, the force-displacement curves of the processed samples were erroneous due to the excessive friction between the ram and the inner surfaces to the channel. The issue was solved later when the sides of the ram were milled, resulting in correct load-displacement curves. One of the ways to improve the design of the billet die would be to add a 2^{o} taper along the vertical channel in order to reduce the friction with the ram as shown in Figure 4.1. Another change would be to have a similar taper along the end of the horizontal channel in order to facilitate the extraction of the extruded sample.

Figure 4.2 suggests an improved mounting setup for the die as the previous one presented some alignment and fitting challenges.

4.2. ECAP Sheet Setup

4.2.1. Initial Design

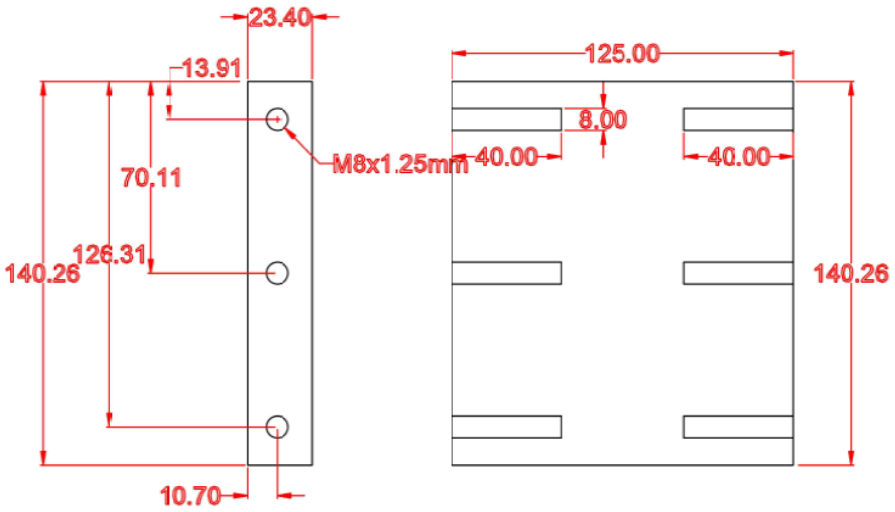

Figure 4.3: Back Plate of the Sheet Die.

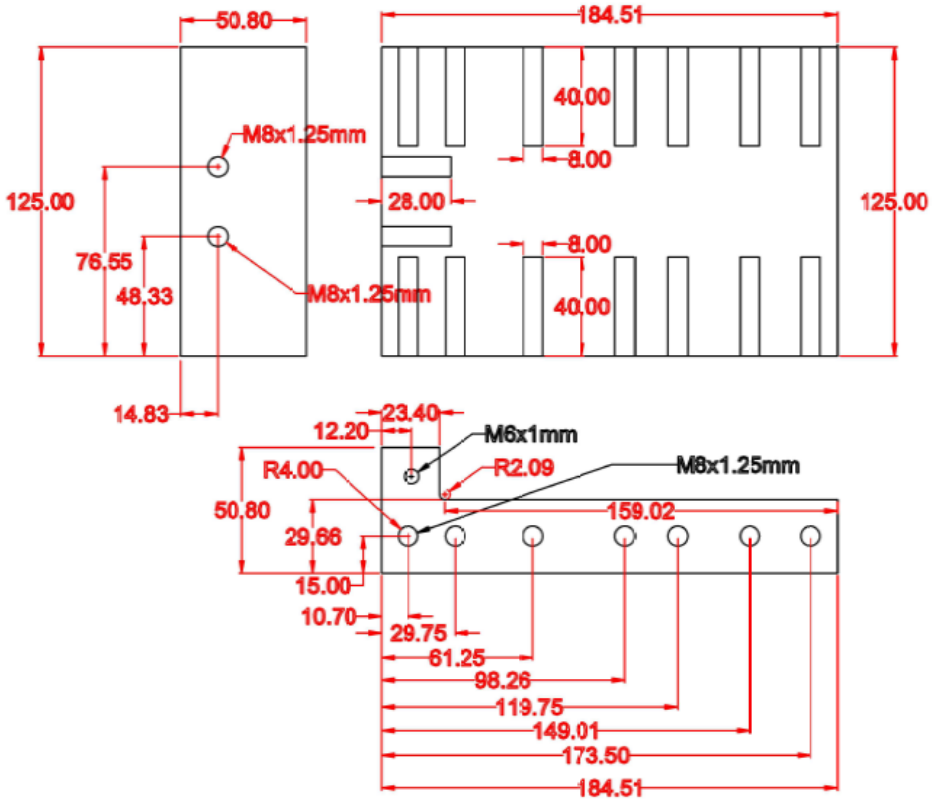

Figure 4.4: Bottom Plate of the Sheet Die.

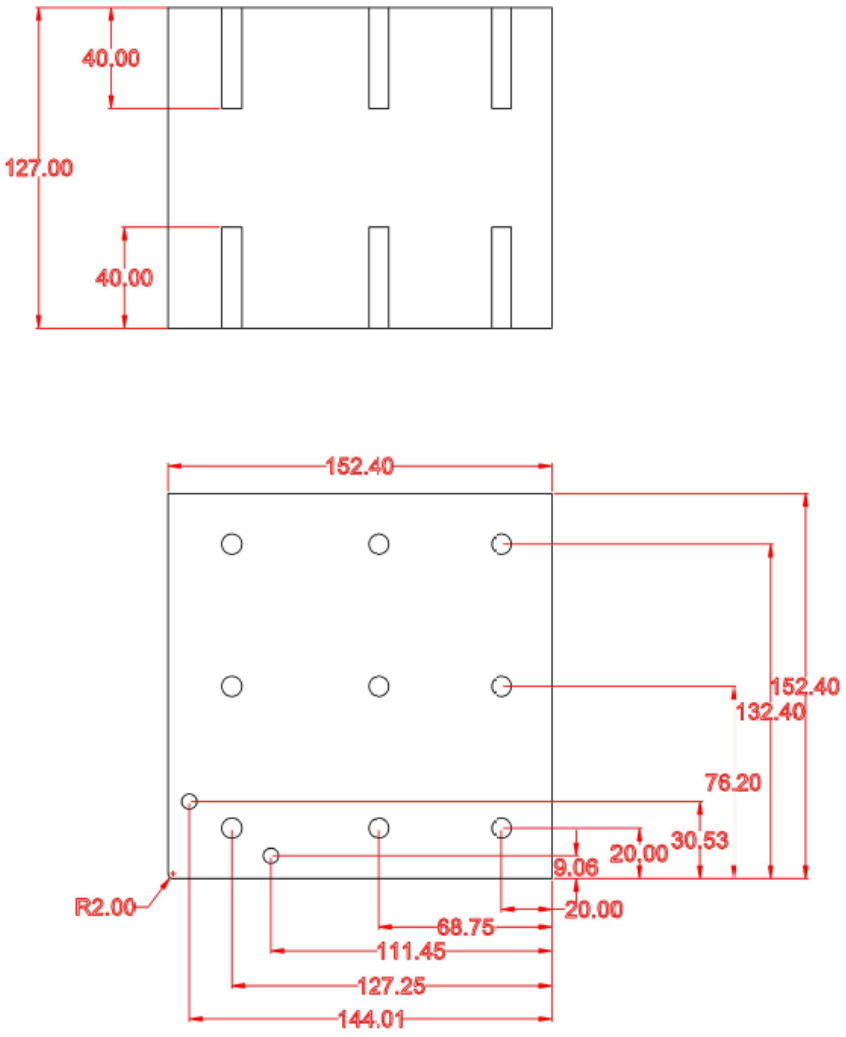

Figure 4.5: Middle Box of the Sheet Die.

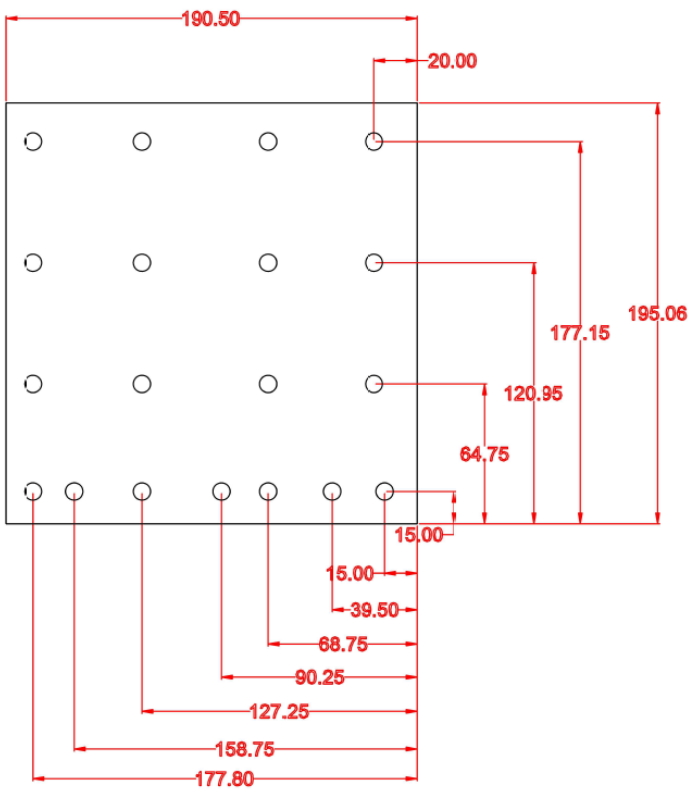

Figure 4.6: Side Clamping Plates of the sheet die.

A special ECAP setup was designed to process sheets of 5” width, 5” length and ½” thickness.

The setup has five different components:

1. The back (Figure 4.3) and bottom (Figure 4.4) die plates that form the outer surface of the ECAP channel.
2. The middle box (Figure 4.5) forming the inner surface of the ECAP channel.
3. Two side clamping plates (Figure 4.6) through which the die is mounted to the base plate and the different components are assembled together.

The assembly of the setup is shown Figure 4.7. The die was made of 304 Stainless Steel purchased from McMaster© and manufactured by the UM-Dearborn machine shops.

A height adjustment plate (Figure 4.8) was manufactured to account for the height differences between the die and the pneumatic cylinder. Proper attachments were designed for the ram adapter (Figure 4.9) and the pneumatic cylinder adapter (Figure 4.10) in order to effectively extrude the sample and apply a back-pressure.

The setup was not used due to the unavailability of the proper equipment to be mounted on.

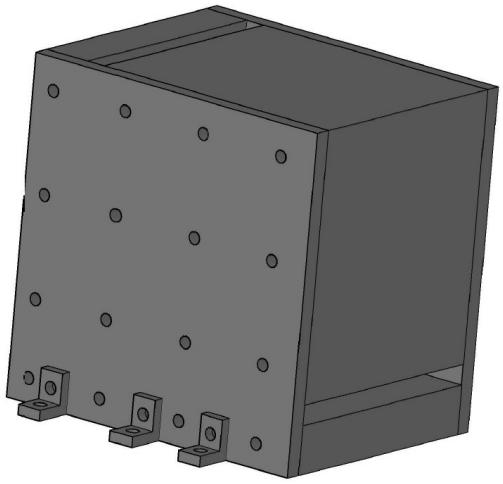

Figure 4.7: Post-manufacturing ECAP Sheets setup.

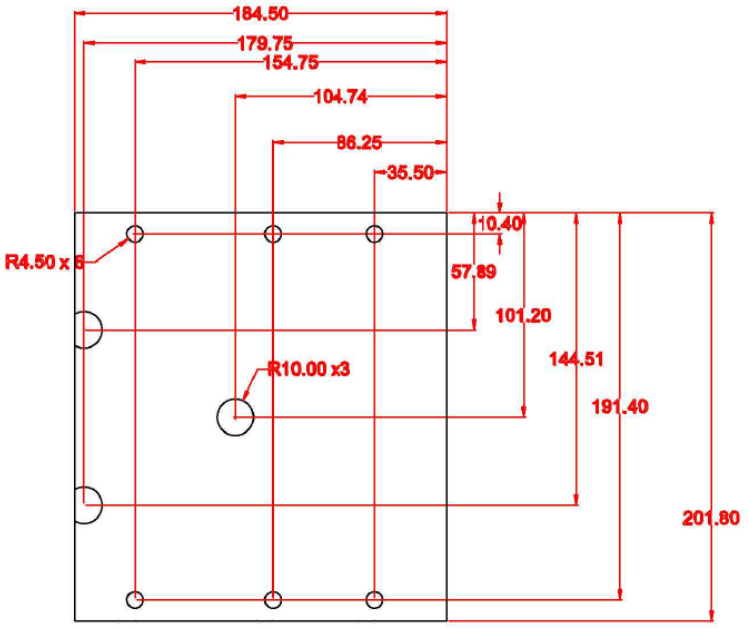

Figure 4.8: Height Adjustment Plate for the Sheets Die.

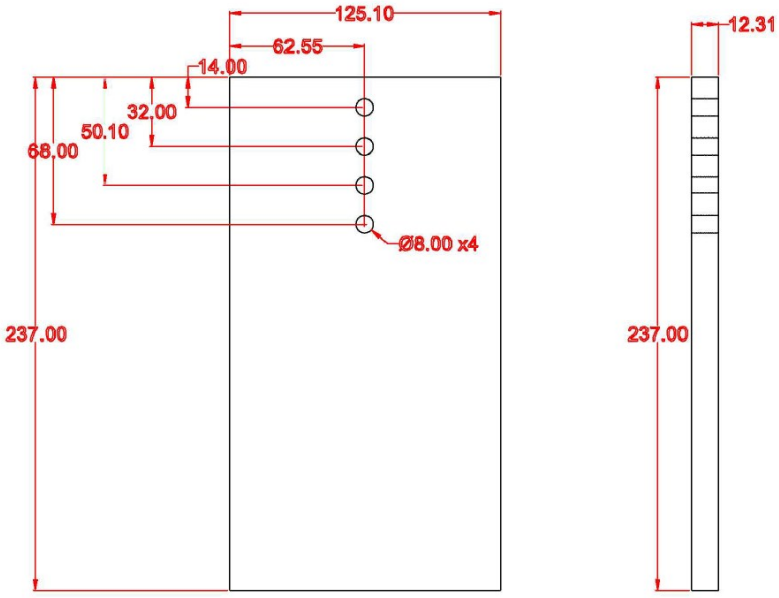

Figure 4.9: Ram Extension Plate.

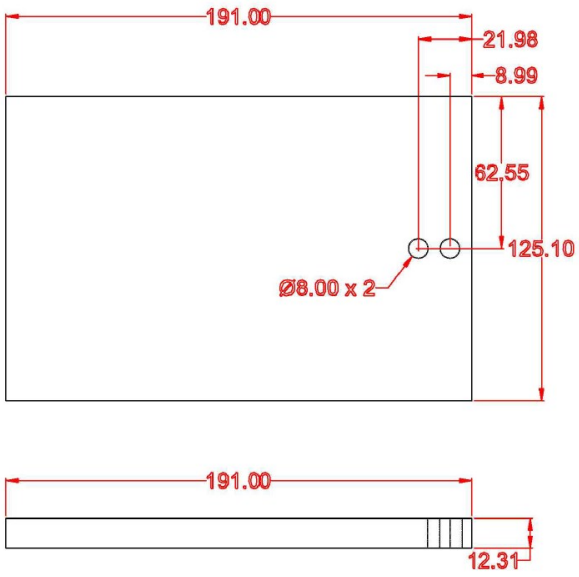

Figure 4.10: Pneumatic Cylinder Extension.

4.2.2. Recommended adjustments

One of the adjustments to the setup would be to change the mounting L-shaped channel in order to improve the alignment and add rigidity to the setup as shown in Figure 4.11.

The ECAP Sheets setup is composed of too many parts for cost reduction purposes, increasing the imperfections in the die and making the alignment of the different plates more challenging. Reducing the overall number of plates by merging both the bottom and the back plates as shown in Figure 4.12 would be a way to solve the encountered issues. An additional reduction to the number of the plates would be to merge the backward clamping plate to the plates shown in the previous figure.

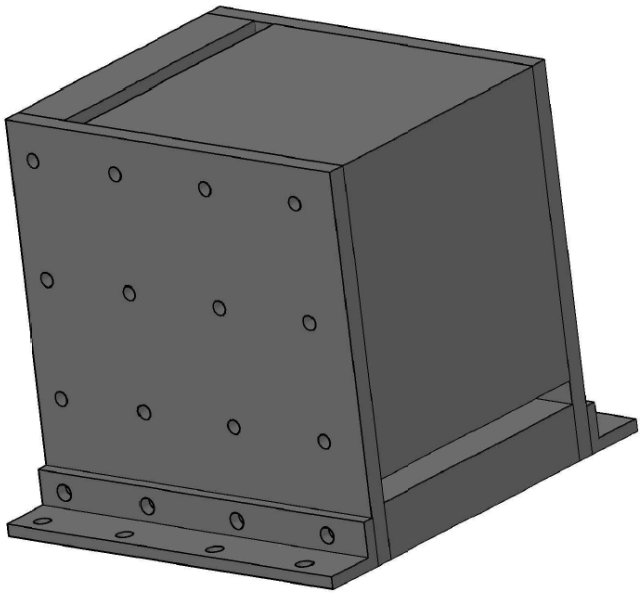

Figure 4.11: Suggested mounting setup for the die.

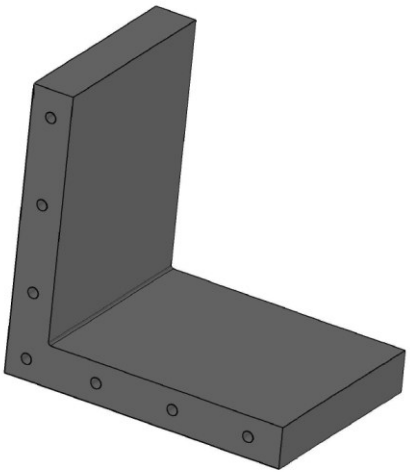

Figure 4.12: Merged bottom and back plates.

4.3. Arcan Testing Setup

4.3.1. Initial Design

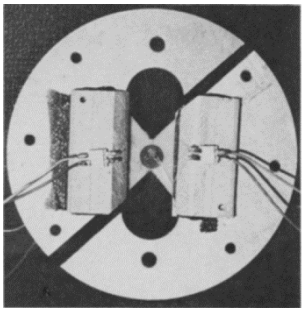

Figure 4.13: Specimen Designed by (Arcan et al., 1978).

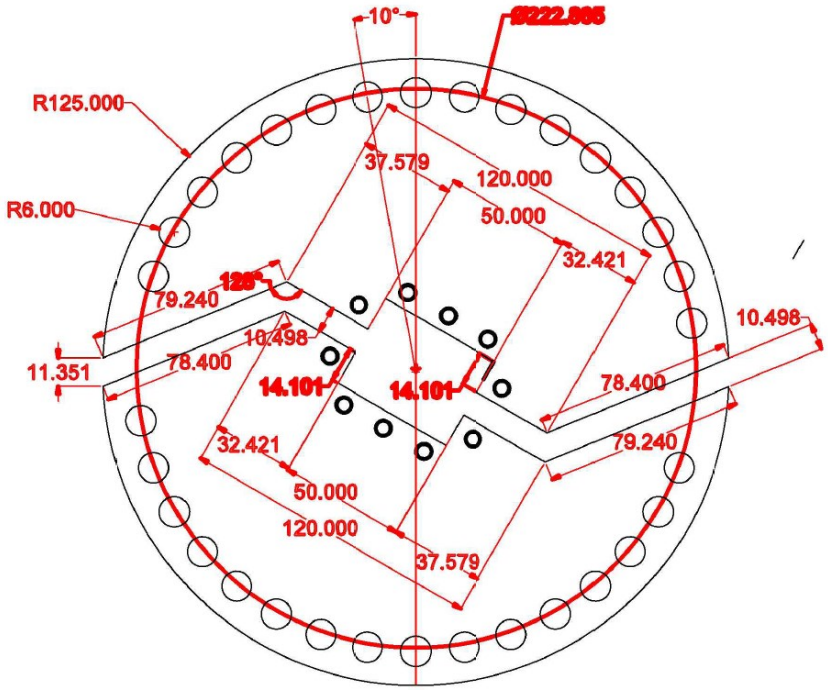

Figure 4.14: Arcan Wheel Design.

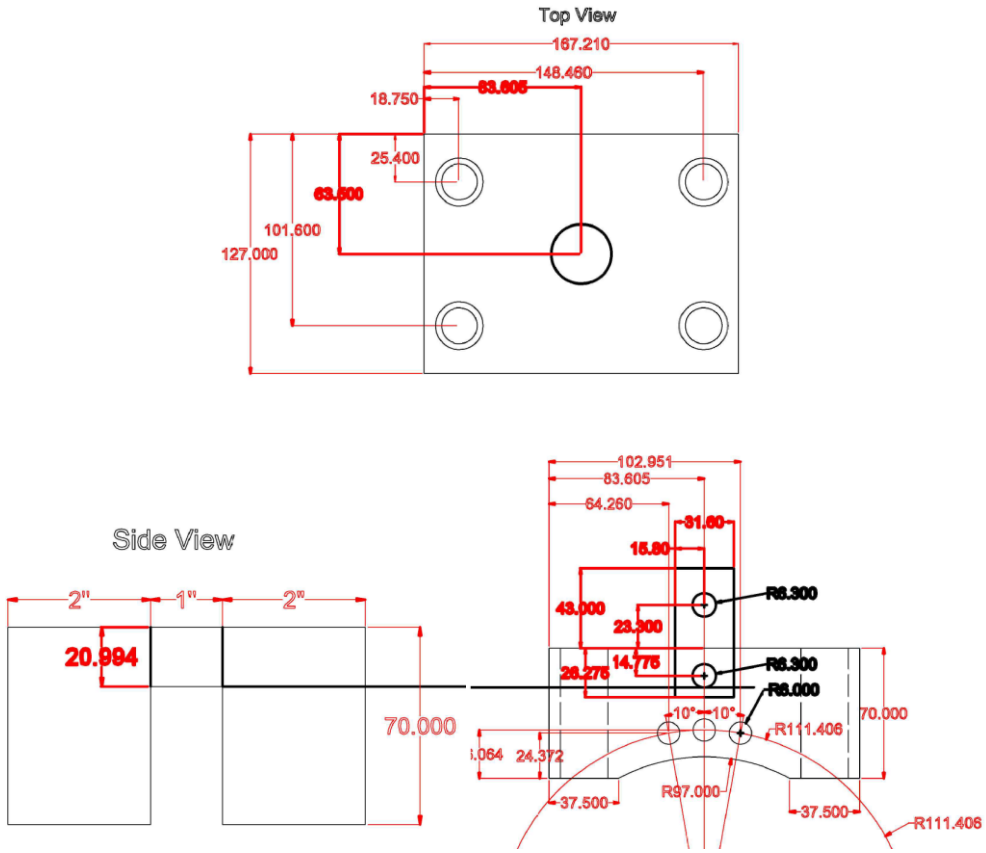

Figure 4.15: Translation Boxes.

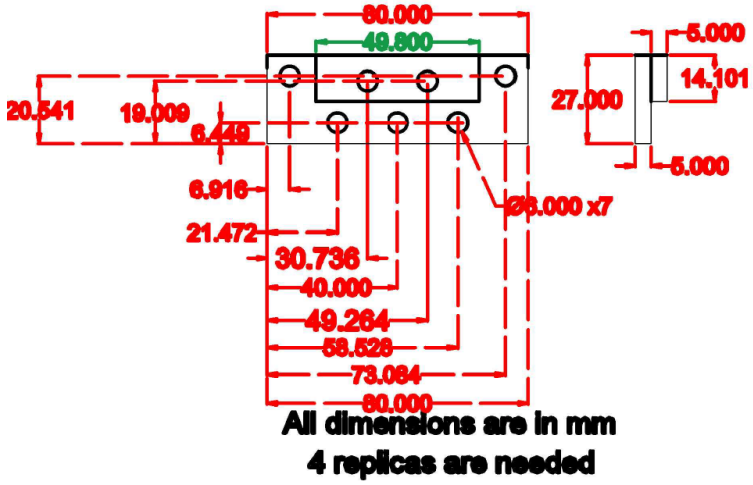

Figure 4.16: Clamping Setups.

Hachour et al., 2014b examined the behavior of high density polyethylene (HDPE) under different stress states. This was achievable through butterfly-shaped specimen mounted on a specifically designed “Arcan Setup”. This setup (Figure 4.13) was designed by Arcan in 1977 as an efficient way to test materials in plane-stress conditions that are able to produce pure shear and normal principal stresses of different signs and arbitrary ratios. While many studies have been conducted to study the tensile properties of thermoplastics, only few studies considered the directionality in the mechanical behavior of thermoplastic polymers.

A new and improved design of the Arcan setup shown in was manufactured at the UM-Dearborn machines shops for the purpose of characterizing the directionality in the ECAP-processed sheets. The setup was composed of the following:

1. A rotating wheel (Figure 4.14) composed of two parts.
2. An upper and a lower translation box (Figure 4.15) through which the rotating wheel is attached.
3. Clamps (Figure 4.16) that are used to attach the sample to the setup.
4. Translation bars used to facilitate the movement of the translation boxes and add stability to the system.

An assembly drawing of the setup is shown in Figure 4.17. Due to the inability of successfully processing sheets, the setup was not used.

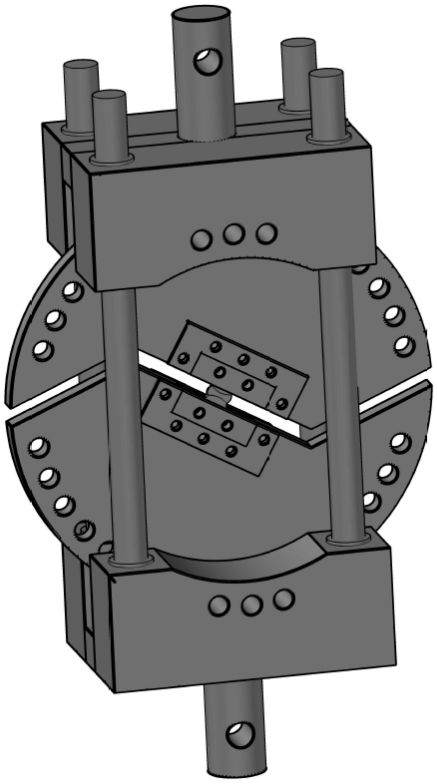

Figure 4.17: Assembly of the Arcan setup.

4.3.2. Recommended Adjustments

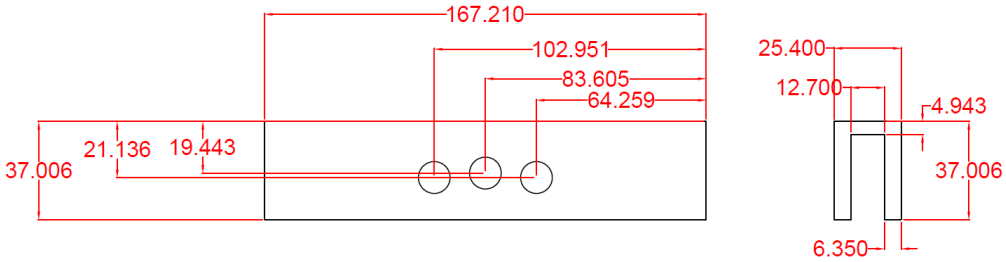

Figure 4.18: Alignmnent Plate for the Arcan Setup.

After manufacturing the Arcan setup, we realized that the upper and lower parts of the wheels need to be properly aligned in order to ensure that the correct forces are applied to the

sample. Two replicates of the suggested plate shown in Figure 4.18 would have to be placed between the wheel and translation boxes to stop any form of possible movement.

4.4. Tensile Testing

The main challenge in the ECAP experiments was to cut the processed billets into tensile specimen. The original plan was to examine the changes of the mechanical properties in the processed samples throughout the thickness, however, the induced samples' curvature after ECAP and the mounting challenges of the sample, resulted in the inability in completing that goal and in reducing the scope to just testing the differences among the samples processed at different conditions.

A diamond blade could not cut any of the three different materials (LDPE, UHMWPE or HDPE). An electroplated blade was finally used that could cut the LDPE and HDPE. There was no available blades that can cut UHMWPE which is why a mechanical characterization of the UHMWPE processed samples could not be conducted.

The thickness of the samples had a consistency problem which could be improved by trying to increase the thickness of the samples and by exploring different cutting setups.

The tensile tests showed obvious trends in regards to the effect of the extrusion velocity and the back-pressure, however, more repetitions are needed to validate the results.

A Digital Image Correlation (DIC) system was used in parallel with the tensile testing, however, one of the main issues was the pealing of the paint at high deformations. Painting the samples and testing them at the same day is a way to reduce the problem, although the resources are not always available as the painting was done at Ford due to the lack of a painting hood at UM-Dearborn.

4.5. Conclusion

The ECAP parameter optimization of three different types of polyethylene (HDPE, LDPE and UHMWPE) were explored. The extrusion velocity was varied from 0.45mm/min to 45mm/min and the back-pressure was varied from 0N to 1120N. A custom-designed ECAP die was used to perform the experiments, after which, the samples were cut into tensile testing specimen.

Table 4.1: Percentage change of the different mechanical properties with the increase of the back-pressure from 0N to 1120N averaged on all tested extrusion velocities and strain rates.

	LDPE	HDPE
Yield Strength (MPa)	-7.69%	-28.04%
Total Strain to Fracture	+85.66%	-45.06%
Modulus of Elasticity (MPa)	-22.46%	-30.46%

Table 4.1 represents the percentage change of the different mechanical properties of the ECAP-processed samples with the increase of the back-pressure from 0N to 1120N averaged on all tested extrusion velocities and strain rates. With the increase of the back-pressure from 0N to 1120N, the yield strength decreased on average by 7.69% for LDPE while it decreased for 28.04% for HDPE. The total strain to fracture reported very different behaviors for both crystallinities of polyethylene: on average, the total strain to fracture increased by 85.66% for LDPE with the increase of the back-pressure from 0N to 1120N while a decrease was reported by 45.06% for the HDPE. The modulus of elasticity decreased for both LDPE and HDPE at comparable levels of 22.46% and 30.46% respectively.

Table 4.2: Percentage change of the different mechanical properties with the increase of the extrusion velocity averaged on all tested back-pressures and strain rates.

	LDPE	HDPE
Yield Strength (MPa)	+7.148%	-1.35%
Total Strain to Fracture	+10.95%	-17.25%
Modulus of Elasticity (MPa)	+9.34%	-5.06%

Table 4.2 represents the percentage change of the different mechanical properties of the ECAP-processed samples with the increase of the extrusion velocity averaged on all the tested back-pressures and strain rates. The increase of the extrusion velocity from 4.5mm/min to 45mm/min increased the yield strength of the LDPE processed samples by only 7.48% averaged for all the tested back-pressures and strain rates and decreased the yield strength of the HDPE samples by 1.35% on average. The increase of velocity had opposite effects on the total strain to fracture which increased by 10.95% on average for LDPE and decreased by 17.25% for HDPE. The modulus of elasticity changed in a similar manner as well: a 9.34% of increase was reported for LDPE and a 5.06% average decrease was reported for HDPE.

Although some general trends have been identified through the presented results regarding the effect of ECAP processing parameters on both LDPE and HDPE, some of the key takeaways of this study include:

- Additional experiments need to be conducted in order to confirm the trends' repeatability by having at least four repetitions per condition.

- The preparation of the testing specimen was the major shortcoming of the current study. Exploring better ways to cut the samples into layers is a necessity to be able to reach better results.
- An improved version of the billet die needs to be manufactured according to the suggested designs in section 4.1. Some experimental issues were faced with the current setup, appropriate fixes and improvements were suggested in order to improve its rigidity and reliability.
- In order to have the sheets die operational and be able to expand the ECAP study on PE, two main options are available: either reduce the size of the current die to fit on the Interlaken press in the Metal Forming Lab or search for another press with a total stroke of at least 5 inches. A method to cut the processed sheets into layers would also need to be explored. Manufacturing the alignment plate of the Arcan setup is enough to make it fully operational.

References

Abdul-Hameed, H., Messager, T., Ayoub, G., Zaïri, F., Naït-Abdelaziz, M., Qu, Z., Zaïri, F., 2014. A two-phase hyperelastic-viscoplastic constitutive model for semi-crystalline polymers: Application to polyethylene materials with a variable range of crystal fractions. J. Mech. Behav. Biomed. Mater. 37, 323–332. https://doi.org/10.1016/J.JMBBM.2014.04.016

Abdul-Hameed, H., Messager, T., Zaïri, F., Naït-Abdelaziz, M., 2014. Large-strain viscoelastic–viscoplastic constitutive modeling of semi-crystalline polymers and model identification by deterministic/evolutionary approach. Comput. Mater. Sci. 90, 241–252. https://doi.org/10.1016/J.COMMATSCI.2014.03.043

Adams, A.M., Buckley, C.P., Jones, D.P., 2000. Biaxial hot drawing of poly(ethylene terephthalate): measurements and modelling of strain-stiffening. Polymer (Guildf). 41, 771–786. https://doi.org/10.1016/S0032-3861(98)00834-9

Ahzi, S., Makradi, A., Gregory, R.V., Edie, D.D., 2003. Modeling of deformation behavior and strain-induced crystallization in poly(ethylene terephthalate) above the glass transition temperature. Mech. Mater. 35, 1139–1148. https://doi.org/10.1016/S0167-6636(03)00004-8

Ames, N.M., Srivastava, V., Chester, S.A., Anand, L., 2009. A thermo-mechanically coupled theory for large deformations of amorphous polymers. Part II: Applications. Int. J. Plast. 25, 1495–1539. https://doi.org/10.1016/J.IJPLAS.2008.11.005

Anand, L., Ames, N.M., Srivastava, V., Chester, S.A., 2009. A thermo-mechanically coupled theory for large deformations of amorphous polymers. Part I: Formulation. Int. J. Plast. 25, 1474–1494. https://doi.org/10.1016/J.IJPLAS.2008.11.004

Anand, L., Gurtin, M.E., 2003. A theory of amorphous solids undergoing large deformations, with application to polymeric glasses. Int. J. Solids Struct. 40, 1465–1487. https://doi.org/10.1016/S0020-7683(02)00651-0

Andrew Phillips, *, Peng-wei Zhu, and, Edward, G., 2006. Simple Shear Deformation of Polypropylene via the Equal Channel Angular Extrusion Process. Macromolecules. 39 (17), 5796–5803. https://doi.org/10.1021/MA0607618

Aour, B., Mitsak, A., 2016. Analysis of plastic deformation of semi-crystalline polymers during ECAE process using 135° die. J. Theor. Appl. Mech. 54, 263. https://doi.org/10.15632/jtam-pl.54.1.263

Aour, B., Zaïri, F., Naït-Abdelaziz, M., Gloaguen, J.M., Lefebvre, J.M., 2009. Finite Element Analysis of Plastic Strain Distribution in Multipass ECAE Process of High Density Polyethylene. J. Manuf. Sci. Eng. 131, 031016. https://doi.org/10.1115/1.3139217

Aour, B., Zaïri, F., Naït-Abdelaziz, M., Gloaguen, J.M., Rahmani, O., Lefebvre, J.M., 2008. A computational study of die geometry and processing conditions effects on equal channel angular extrusion of a polymer. Int. J. Mech. Sci. 50, 589–602. https://doi.org/10.1016/J.IJMECSCI.2007.07.012

Arcan, M., Hashin, Z., Voloshin, A., 1978. A method to produce uniform plane-stress states with applications to fiber-reinforced materials. Exp. Mech. 18, 141–146. https://doi.org/10.1007/BF02324146

Arruda, E.M., Boyce, M.C., 1993. A three-dimensional constitutive model for the large stretch behavior of rubber elastic materials. J. Mech. Phys. Solids 41, 389–412. https://doi.org/10.1016/0022-5096(93)90013-6

Arruda, E.M., Boyce, M.C., Jayachandran, R., 1995. Effects of strain rate, temperature and thermomechanical coupling on the finite strain deformation of glassy polymers. Mech. Mater. 19, 193–212. https://doi.org/10.1016/0167-6636(94)00034-E

Ayoub, G., Zaïri, F., Fréderix, C., Gloaguen, J.M., Naït-Abdelaziz, M., Seguela, R., Lefebvre, J.M., 2011a. Effects of crystal content on the mechanical behaviour of polyethylene under finite strains: Experiments and constitutive modelling. Int. J. Plast. 27, 492–511. https://doi.org/10.1016/J.IJPLAS.2010.07.005

Ayoub, G., Zaïri, F., Naït-Abdelaziz, M., Gloaguen, J.M., 2011b. Modeling the low-cycle fatigue behavior of visco-hyperelastic elastomeric materials using a new network alteration theory: Application to styrene-butadiene rubber. J. Mech. Phys. Solids 59, 473–495. https://doi.org/10.1016/J.JMPS.2010.09.016

Ayoub, G., Zaïri, F., Naït-Abdelaziz, M., Gloaguen, J.M., 2010. Modelling large deformation behaviour under loading–unloading of semicrystalline polymers: Application to a high density polyethylene. Int. J. Plast. 26, 329–347. https://doi.org/10.1016/J.IJPLAS.2009.07.005

Bardenhagen, S.G., Stout, M.G., Gray, G.T., 1997. Three-dimensional, finite deformation, viscoplastic constitutive models for polymeric materials. Mech. Mater. 25, 235–253. https://doi.org/10.1016/S0167-6636(97)00007-0

Bartczak, Z., 2005. Influence of molecular parameters on high-strain deformation of polyethylene in the plane-strain compression. Part II. Strain recovery. Polymer (Guildf). 46, 10339–10354. https://doi.org/10.1016/J.POLYMER.2005.07.096

Bartczak, Z., Argon, A.S., Cohen, R.E., 1994. Texture evolution in large strain simple shear deformation of high density polyethylene. Polymer (Guildf). 35, 3427–3441.

https://doi.org/10.1016/0032-3861(94)90905-9

Bartczak, Z., Galeski, A., 2010a. Plasticity of Semicrystalline Polymers. Macromol. Symp. 294, 67–90. https://doi.org/10.1002/masy.201050807

Bartczak, Z., Galeski, A., 2010b. Plasticity of Semicrystalline Polymers. Macromol. Symp. 294, 67–90. https://doi.org/10.1002/masy.201050807

Belbachir, S., Zaïri, F., Ayoub, G., Maschke, U., Naït-Abdelaziz, M., Gloaguen, J.M., Benguediab, M., Lefebvre, J.M., 2010. Modelling of photodegradation effect on elastic–viscoplastic behaviour of amorphous polylactic acid films. J. Mech. Phys. Solids 58, 241–255. https://doi.org/10.1016/J.JMPS.2009.10.003

Beloshenko, V.A., Voznyak, Y. V., Reshidova, I.Y., Naït-Abdelaziz, M., Zairi, F., 2013. Equal-channel angular extrusion of polymers. J. Polym. Res. 20, 322. https://doi.org/10.1007/s10965-013-0322-2

Beloshenko, V.A., Voznyak, Y. V, Reshidova, I.Y., Naït-Abdelaziz, M., Zairi, F., 2013. Equal-channel angular extrusion of polymers. https://doi.org/10.1007/s10965-013-0322-2

Ben Hadj Hamouda, H., Laiarinandrasana, L., Piques, R., 2007. Viscoplastic behaviour of a medium density polyethylene (MDPE): Constitutive equations based on double nonlinear deformation model. Int. J. Plast. 23, 1307–1327. https://doi.org/10.1016/J.IJPLAS.2006.11.007

Berbon, P.B., Furukawa, M., Horita, Z., Nemoto, M., Langdon, T.G., 1999a. Influence of pressing speed on microstructural development in equal-channel angular pressing. Metall. Mater. Trans. A 30, 1989–1997. https://doi.org/10.1007/s11661-999-0009-9

Berbon, P.B., Furukawa, M., Horita, Z., Nemoto, M., Langdon, T.G., 1999b. Influence of pressing speed on microstructural development in equal-channel angular pressing. Metall. Mater. Trans. A 30, 1989–1997. https://doi.org/10.1007/s11661-999-0009-9

Bouaksa, F., Ovalle Rodas, C., Zaïri, F., Stoclet, G., Naït-Abdelaziz, M., Gloaguen, J.M., Tamine, T., Lefebvre, J.M., 2014. Molecular chain orientation in polycarbonate during equal channel angular extrusion: Experiments and simulations. Comput. Mater. Sci. 85, 244–252. https://doi.org/10.1016/J.COMMATSCI.2013.12.028

Boulahia, R., Gloaguen, J.M., Zaïri, F., Naït-Abdelaziz, M., Seguela, R., Boukharouba, T., Lefebvre, J.M., 2009. Deformation behaviour and mechanical properties of polypropylene processed by equal channel angular extrusion: Effects of back-pressure and extrusion velocity. Polymer (Guildf). 50, 5508–5517. https://doi.org/10.1016/J.POLYMER.2009.09.050

Bowen, J.R., Gholinia, A., Roberts, S.M., Prangnell, P.B., 2000. Analysis of the billet deformation behaviour in equal channel angular extrusion. Mater. Sci. Eng. A 287, 87–99.

https://doi.org/10.1016/S0921-5093(00)00834-0

Boyce, M.C., Parks, D.M., Argon, A.S., 1988. Large inelastic deformation of glassy polymers. part I: rate dependent constitutive model. Mech. Mater. 7, 15–33. https://doi.org/10.1016/0167-6636(88)90003-8

Brooks, N.W.J., Duckett, R.A., Ward, I.M., 1998. Temperature and strain-rate dependence of yield stress of polyethylene. J. Polym. Sci. Part B Polym. Phys. 36, 2177–2189. https://doi.org/10.1002/(SICI)1099-0488(19980915)36:12<2177::AID-POLB15>3.0.CO;2-X

Brown, N., Ward, I.M., 1983. The influence of morphology and molecular weight on ductile-brittle transitions in linear polyethylene. J. Mater. Sci. 18, 1405–1420. https://doi.org/10.1007/BF01111960

Buckley, C.P., Jones, D.C., 1995. Glass-rubber constitutive model for amorphous polymers near the glass transition. Polymer (Guildf). 36, 3301–3312. https://doi.org/10.1016/0032-3861(95)99429-X

Callister, W.D., 1997. Materials science and engineering : an introduction. John Wiley & Sons.

Campbell, B., Edward, G., 1999. Equal channel angular extrusion of polyalkenes. Plast. Rubber Compos. 28, 467–475. https://doi.org/10.1179/146580199101540033

Chen, Y.C., Huang, Y.Y., Chang, C.P., Kao, P.W., 2003. The effect of extrusion temperature on the development of deformation microstructures in 5052 aluminium alloy processed by equal channel angular extrusion. Acta Mater. 51, 2005–2015. https://doi.org/10.1016/S1359-6454(02)00607-9

Chung, S.W., Somekawa, H., Kinoshita, T., Kim, W.J., Higashi, K., 2004. The non-uniform behavior during ECAE process by 3-D FVM simulation. Scr. Mater. 50, 1079–1083. https://doi.org/10.1016/J.SCRIPTAMAT.2003.11.062

Colak, O.U., 2005. Modeling deformation behavior of polymers with viscoplasticity theory based on overstress. Int. J. Plast. 21, 145–160. https://doi.org/10.1016/J.IJPLAS.2004.04.004

Creasy, T.S., Kang, Y.S., 2005. Fibre fracture during equal-channel angular extrusion of short fibre-reinforced thermoplastics. J. Mater. Process. Technol. 160, 90–98. https://doi.org/10.1016/J.JMATPROTEC.2004.04.369

DeLo, D.P., Semiatin, S.L., 1999. Finite-element modeling of nonisothermal equal-channel angular extrusion. Metall. Mater. Trans. A 30, 1391–1402. https://doi.org/10.1007/s11661-999-0287-2

Drozdov, A.D., 2009. Mullins' effect in semicrystalline polymers. Int. J. Solids Struct. 46, 3336–

3345. https://doi.org/10.1016/J.IJSOLSTR.2009.05.001

Dupaix, R.B., Krishnan, D., 2006. A Constitutive Model for Strain-Induced Crystallization in Poly(ethylene terephthalate) (PET) during Finite Strain Load-Hold Simulations. J. Eng. Mater. Technol. 128, 28. https://doi.org/10.1115/1.1924564

Dusunceli, N., Colak, O.U., 2008. Modelling effects of degree of crystallinity on mechanical behavior of semicrystalline polymers. Int. J. Plast. 24, 1224–1242. https://doi.org/10.1016/J.IJPLAS.2007.09.003

Elmeguenni, M., Naït-Abdelaziz, M., Zaïri, F., Gloaguen, J.M., 2013. Fracture characterization of high-density polyethylene pipe materials using the $$J$$ J -integral and the essential work of fracture. Int. J. Fract. 183, 119–133. https://doi.org/10.1007/s10704-013-9848-x

Ferrasse, S., Segal, V.M., Alford, F., Kardokus, J., Strothers, S., 2008. Scale up and application of equal-channel angular extrusion for the electronics and aerospace industries. Mater. Sci. Eng. A 493, 130–140. https://doi.org/10.1016/J.MSEA.2007.04.133

Furukawa, M., Horita, Z., Langdon, T.G., 2003. Factors influencing microstructural development in equal-channel angular pressing. Met. Mater. Int. 9, 141–149. https://doi.org/10.1007/BF03027270

Furukawa, M., Horita, Z., Nemoto, M., Langdon, T.G., 2001. Review: Processing of metals by equal-channel angular pressing. J. Mater. Sci. 36, 2835–2843. https://doi.org/10.1023/A:1017932417043

Furukawa, M., Horita, Z., Nemoto, M., Langdon, T.G., 2001. Review: Processing of metals by equal-channel angular pressing. J. Mater. Sci. 36, 2835–2843. https://doi.org/10.1023/a:1017932417043

Furuno, K., Akamatsu, H., Oh-ishi, K., Furukawa, M., Horita, Z., Langdon, T.G., 2004. Microstructural development in equal-channel angular pressing using a 60° die. Acta Mater. 52, 2497–2507. https://doi.org/10.1016/J.ACTAMAT.2004.01.040

Gholinia, A., Prangnell, P.B., Markushev, M.V., 2000. The effect of strain path on the development of deformation structures in severely deformed aluminium alloys processed by ECAE. Acta Mater. 48, 1115–1130. https://doi.org/10.1016/S1359-6454(99)00388-2

Ghorbel, E., 2008. A viscoplastic constitutive model for polymeric materials. Int. J. Plast. 24, 2032–2058. https://doi.org/10.1016/J.IJPLAS.2008.01.003

Hachour, K., Zaïri, F., Naït-Abdelaziz, M., Gloaguen, J.M., Aberkane, M., Lefebvre, J.M., 2014a. Experiments and modeling of high-crystalline polyethylene yielding under different stress states. Int. J. Plast. 54, 1–18. https://doi.org/10.1016/J.IJPLAS.2013.06.004

Hachour, K., Zaïri, F., Naït-Abdelaziz, M., Gloaguen, J.M., Aberkane, M., Lefebvre, J.M.,

2014b. Experiments and modeling of high-crystalline polyethylene yielding under different stress states. Int. J. Plast. 54, 1–18. https://doi.org/10.1016/J.IJPLAS.2013.06.004

Hachour, K., Zaïri, F., Naït-Abdelaziz, M., Gloaguen, J.M., Aberkane, M., Lefebvre, J.M., 2014c. Experiments and modeling of high-crystalline polyethylene yielding under different stress states. Int. J. Plast. 54, 1–18. https://doi.org/10.1016/J.IJPLAS.2013.06.004

Haward, R.., Thackray, G., 1968. The Use of a Mathematical Model to Describe Isothermal Stress-Strain Curves in Glassy Thermoplastics on JSTOR. Proc. R. Soc. London 302, 453–472.

Horie, K., Barón, M., Fox, R.B., He, J., Hess, M., Kahovec, J., Kitayama, T., Kubisa, P., Maréchal, E., Mormann, W., Stepto, R.F.T., Tabak, D., Vohlídal, J., Wilks, E.S., Work, W.J., 2004. Definitions of terms relating to reactions of polymers and to functional polymeric materials (IUPAC Recommendations 2003). Pure Appl. Chem. 76, 889–906. https://doi.org/10.1351/pac200476040889

Horita, Z., Furukawa, M., Nemoto, M., Langdon, T.G., 2000. Development of fine grained structures using severe plastic deformation. Mater. Sci. Technol. 16, 1239–1245. https://doi.org/10.1179/026708300101507091

Huang, W.H., Chang, L., Kao, P.W., Chang, C.P., 2001. Effect of die angle on the deformation texture of copper processed by equal channel angular extrusion. Mater. Sci. Eng. A 307, 113–118. https://doi.org/10.1016/S0921-5093(00)01881-5

Huang, W.H., Yu, C.Y., Kao, P.W., Chang, C.P., 2004. The effect of strain path and temperature on the microstructure developed in copper processed by ECAE. Mater. Sci. Eng. A 366, 221–228. https://doi.org/10.1016/J.MSEA.2003.08.033

Iwahashi, Y., Furukawa, M., Horita, Z., Nemoto, M., Langdon, T.G., 1998. Microstructural characteristics of ultrafine-grained aluminum produced using equal-channel angular pressing. Metall. Mater. Trans. A 29, 2245–2252. https://doi.org/10.1007/s11661-998-0102-5

Iwahashi, Y., Wang, J., Horita, Z., Nemoto, M., Langdon, T.G., 1996. Principle of equal-channel angular pressing for the processing of ultra-fine grained materials. Scr. Mater. 35, 143–146. https://doi.org/10.1016/1359-6462(96)00107-8

Jenkins, A.D., Kratochvíl, P., Stepto, R.F.T., Suter, U.W., 1996. Glossary of basic terms in polymer science (IUPAC Recommendations 1996). Pure Appl. Chem. 68, 2287–2311. https://doi.org/10.1351/pac199668122287

Kamachi, M., Furukawa, M., Horita, Z., Langdon, T.G., 2003. Equal-channel angular pressing using plate samples. Mater. Sci. Eng. A 361, 258–266. https://doi.org/10.1016/S0921-5093(03)00522-7

Kazmierczak, T., Galeski, A., Argon, A.S., 2005. Plastic deformation of polyethylene crystals as a function of crystal thickness and compression rate. Polymer (Guildf). 46, 8926–8936. https://doi.org/10.1016/J.POLYMER.2005.06.073

Khan, A., Zhang, H., 2001. Finite deformation of a polymer: experiments and modeling. Int. J. Plast. 17, 1167–1188. https://doi.org/10.1016/S0749-6419(00)00073-5

Kim, H.S., Hong, S.I., Seo, M.H., 2001. Effects of strain hardenability and strain-rate sensitivity on the plastic flow and deformation homogeneity during equal channel angular pressing. J. Mater. Res. 16, 856–864. https://doi.org/10.1557/JMR.2001.0113

Kim, I., Kim, J., Shin, D.H., Park, K.-T., 2003. Effects of grain size and pressing speed on the deformation mode of commercially pure Ti during equal channel angular pressing. Metall. Mater. Trans. A 34, 1555–1558. https://doi.org/10.1007/s11661-003-0267-x

Lee, S.C., Ha, S.Y., Kim, K.T., Hwang, S.M., Huh, L.M., Chung, H.S., 2004. Finite element analysis for deformation behavior of an aluminum alloy composite containing SiC particles and porosities during ECAP. Mater. Sci. Eng. A 371, 306–312. https://doi.org/10.1016/J.MSEA.2003.12.029

Li, C.K.-Y., Xia, Z.-Y., Sue, H.-J., 2000. Simple shear plastic deformation behavior of polycarbonate plate II. Mechanical property characterization. Polymer (Guildf). 41, 6285–6293. https://doi.org/10.1016/S0032-3861(99)00837-X

Lin, L., Argon, A.S., 1994. Structure and plastic deformation of polyethylene. J. Mater. Sci. 29, 294–323. https://doi.org/10.1007/BF01162485

Makki, M., Ayoub, G., Abdul-Hameed, H., Zaïri, F., Mansoor, B., Naït-Abdelaziz, M., Ouederni, M., 2017. Mullins effect in polyethylene and its dependency on crystal content: A network alteration model. J. Mech. Behav. Biomed. Mater. 75, 442–454. https://doi.org/10.1016/J.JMBBM.2017.04.022

Makradi, A., Ahzi, S., Gregory, R.V., Edie, D.D., 2005. A two-phase self-consistent model for the deformation and phase transformation behavior of polymers above the glass transition temperature: application to PET. Int. J. Plast. 21, 741–758. https://doi.org/10.1016/J.IJPLAS.2004.04.012

Nakashima, K., Horita, Z., Nemoto, M., Langdon, T.G., 1998. Influence of channel angle on the development of ultrafine grains in equal-channel angular pressing. Acta Mater. 46, 1589–1599. https://doi.org/10.1016/S1359-6454(97)00355-8

Pampillo, C.A., Davis, L.A., 1972a. Temperature dependence of the yield and flow stresses of linear high-molecular-weight polyethylene. J. Appl. Phys. 43, 4277–4285. https://doi.org/10.1063/1.1660917

Pampillo, C.A., Davis, L.A., 1972b. Temperature dependence of the yield and flow stresses of

linear high-molecular-weight polyethylene. J. Appl. Phys. 43, 4277–4285. https://doi.org/10.1063/1.1660917

Park, J.-W., Suh, J.-Y., 2001. Effect of die shape on the deformation behavior in equal-channel angular pressing. Metall. Mater. Trans. A 32, 3007–3014. https://doi.org/10.1007/s11661-001-0175-x

Patlazhan, S., Remond, Y., 2012. Structural mechanics of semicrystalline polymers prior to the yield point: a review. J. Mater. Sci. 47, 6749–6767. https://doi.org/10.1007/s10853-012-6620-y

Peacock, A.J., 2000. Handbook of polyethylene; structures, properties, and applications. Marcel Dekker, Portland, OR.

Pei, Q.X., Hu, B.H., Lu, C., Wang, Y.Y., 2003. A finite element study of the temperature rise during equal channel angular pressing. Scr. Mater. 49, 303–308. https://doi.org/10.1016/S1359-6462(03)00284-7

Perig, A. V., Golodenko, N.N., 2014. CFD Simulation of ECAE through a multiple-angle die with a movable inlet wall. Chem. Eng. Commun. 201, 1221–1239. https://doi.org/10.1080/00986445.2014.894509

Perig, A. V., Laptev, A.M., Golodenko, N.N., Erfort, Y.A., Bondarenko, E.A., 2010. Equal channel angular extrusion of soft solids. Mater. Sci. Eng. A 527, 3769–3776. https://doi.org/10.1016/J.MSEA.2010.03.043

Prangnell, P.B., Harris, C., Roberts, S.M., 1997. Finite element modelling of equal channel angular extrusion. Scr. Mater. 37, 983–989. https://doi.org/10.1016/S1359-6462(97)00192-9

Regrain, C., Laiarinandrasana, L., Toillon, S., Saï, K., 2009. Multi-mechanism models for semi-crystalline polymer: Constitutive relations and finite element implementation. Int. J. Plast. 25, 1253–1279. https://doi.org/10.1016/J.IJPLAS.2008.09.010

Richeton, J., Ahzi, S., Vecchio, K.S., Jiang, F.C., Adharapurapu, R.R., 2006. Influence of temperature and strain rate on the mechanical behavior of three amorphous polymers: Characterization and modeling of the compressive yield stress. Int. J. Solids Struct. 43, 2318–2335. https://doi.org/10.1016/J.IJSOLSTR.2005.06.040

Richeton, J., Ahzi, S., Vecchio, K.S., Jiang, F.C., Makradi, A., 2007. Modeling and validation of the large deformation inelastic response of amorphous polymers over a wide range of temperatures and strain rates. Int. J. Solids Struct. 44, 7938–7954. https://doi.org/10.1016/J.IJSOLSTR.2007.05.018

Rozanski, A., Galeski, A., 2013. Plastic yielding of semicrystalline polymers affected by amorphous phase. Int. J. Plast. 41, 14–29. https://doi.org/10.1016/J.IJPLAS.2012.07.008

Rubin, Elyse. " The Dissertation Handbook: A Guide to Submitting Your Doctoral Dissertation and Completing Your Doctoral Degree Requirements." Diss. U of Michigan, 2017

Saray, O., Purcek, G., Karaman, I., Neindorf, T., Maier, H.J., 2011. Equal-channel angular sheet extrusion of interstitial-free (IF) steel: Microstructural evolution and mechanical properties. Mater. Sci. Eng. A 528, 6573–6583. https://doi.org/10.1016/J.MSEA.2011.05.014

Seguela, R., ElKoun, S., Seguela, R., 1998a. Plastic deformation of polyethylene and ethylene copolymers: Part II Heterogeneous crystal slip and strain-induced phase change. J. Mater. Sci. 33, 1801–1807. https://doi.org/10.1023/A:1004340902180

Seguela, R., Gaucher-Miri, V., Seguela, R., 1998b. Plastic deformation of polyethylene and ethylene copolymers: Part I Homogeneous crystal slip and molecular mobility. J. Mater. Sci. 33, 1273–1279. https://doi.org/10.1023/A:1004342113141

Semiatin, S.L., DeLo, D.P., Shell, E.B., 2000. The effect of material properties and tooling design on deformation and fracture during equal channel angular extrusion. Acta Mater. 48, 1841–1851. https://doi.org/10.1016/S1359-6454(00)00019-7

Shan, A., Moon, I.-G., Ko, H.-S., Park, J.-W., 1999. Direct observation of shear deformation during equal channel angular pressing of pure aluminum. Scr. Mater. 41, 353–357. https://doi.org/10.1016/S1359-6462(99)00188-8

Shin, D.H., Pak, J.-J., Kim, Y.K., Park, K.-T., Kim, Y.-S., 2002. Effect of pressing temperature on microstructure and tensile behavior of low carbon steels processed by equal channel angular pressing. Mater. Sci. Eng. A 323, 409–415. https://doi.org/10.1016/S0921-5093(01)01395-8

Sue, H.-J., Dilan, H., Li, C.K.-Y., 1999. Simple shear plastic deformation behavior of polycarbonate plate due to the equal channel angular extrusion process. I: Finite element methods modeling. Polym. Eng. Sci. 39, 2505–2515. https://doi.org/10.1002/pen.11638

Sue, H., K.-Y.Li, C., 1998. Control of Orientation of Lamellar Structure in Linear Low Density Polyethylene Via a Novel Equal Channel Angular Extrusion Process. J. Mater. Sci. Lett. 17, 853–856. https://doi.org/10.1023/A:1006659127256

Suh, J., Victoria-Hernandez, J., Letzig, D., Golle, R., Yi, S., Bohlen, J., Volk, W., 2015. Improvement in cold formability of AZ31 magnesium alloy sheets processed by equal channel angular pressing. J. Mater. Process. Technol. 217, 286–293. https://doi.org/10.1016/J.JMATPROTEC.2014.11.029

Tervoort, T.A., Smit, R.J.M., Brekelmans, W.A.M., Govaert, L.E., 1997. A Constitutive Equation for the Elasto-Viscoplastic Deformation of Glassy Polymers. Mech. Time-Dependent Mater. 1, 269–291. https://doi.org/10.1023/A:1009720708029

Valiev, R.Z., Langdon, T.G., 2006. Principles of equal-channel angular pressing as a processing tool for grain refinement. Prog. Mater. Sci. 51, 881–981. https://doi.org/10.1016/J.PMATSCI.2006.02.003

Victoria-Hernández, J., Suh, J., Yi, S., Bohlen, J., Volk, W., Letzig, D., 2016. Strain-induced selective grain growth in AZ31 Mg alloy sheet deformed by equal channel angular pressing. Mater. Charact. 113, 98–107. https://doi.org/10.1016/J.MATCHAR.2016.01.002

Vladimir M. Segal, 2017. 1. Equal Channel Angular Extrusion (ECAE) - Knovel, in: Severe Plastic Deformation Technology. Whittles Publishing.

Wang, T., Tang, S., Chen, J., 2011. Effects of processing route on morphology and mechanical behavior of polypropylene in equal channel angular extrusion. J. Appl. Polym. Sci. 122, 2146–2158. https://doi.org/10.1002/app.34335

Wang, Z.-G., Xia, Z.-Y., Yu, Z.-Q., Chen, E.-Q., Sue, H.-J., Han, C.C., Hsiao, B.S., 2006. Lamellar Formation and Relaxation in Simple Sheared Poly(ethylene terephthalate) by Small-Angle X-ray Scattering. Macromolecules 39, 2930–2939. https://doi.org/10.1021/ma051928k

Weon, J.-I., Sue, H.-J., 2005. Effects of clay orientation and aspect ratio on mechanical behavior of nylon-6 nanocomposite. Polymer (Guildf). 46, 6325–6334. https://doi.org/10.1016/J.POLYMER.2005.05.094

Weon, J.I., Creasy, T.S., Sue, H.-J., Hsieh, A.J., 2005. Mechanical behavior of polymethylmethacrylate with molecules oriented via simple shear. Polym. Eng. Sci. 45, 314–324. https://doi.org/10.1002/pen.20269

Wu, P.D., van der Giessen, E., 1995. On neck propagation in amorphous glassy polymers under plane strain tension. Int. J. Plast. 11, 211–235. https://doi.org/10.1016/0749-6419(94)00043-3

Xia, K., Wu, X., Honma, T., Ringer, S.P., 2007. Ultrafine pure aluminium through back pressure equal channel angular consolidation (BP-ECAC) of particles. J. Mater. Sci. 42, 1551–1560. https://doi.org/10.1007/s10853-006-0819-8

Xia, Z., Sue, H.-J., Hsieh, A.J., 2001a. Impact fracture behavior of molecularly orientated polycarbonate sheets. J. Appl. Polym. Sci. 79, 2060–2066. https://doi.org/10.1002/1097-4628(20010314)79:11<2060::AID-APP1015>3.0.CO;2-E

Xia, Z., Sue, H.-J., Hsieh, A.J., Huang, J.W.-L., 2001b. Dynamic mechanical behavior of oriented semicrystalline polyethylene terephthalate. J. Polym. Sci. Part B Polym. Phys. 39, 1394–1403. https://doi.org/10.1002/polb.1111

Yamaguchi, D., Horita, Z., Nemoto, M., Langdon, T.G., 1999. Significance of adiabatic heating in equal-channel angular pressing. Scr. Mater. 41, 791–796. https://doi.org/10.1016/S1359-

6462(99)00233-X

Yamashita, A., Yamaguchi, D., Horita, Z., Langdon, T.G., 2000. Influence of pressing temperature on microstructural development in equal-channel angular pressing. Mater. Sci. Eng. A 287, 100–106. https://doi.org/10.1016/S0921-5093(00)00836-4

Yoshioka, S., Tsukamoto, K., 2009. Effects of ECAE on Plastic Deformation Behavior of Glassy Polymers. J. Soc. Mater. Sci. Japan 58, 29–34. https://doi.org/10.2472/jsms.58.29

Young, R.J. (Robert J., 1981. Introduction to polymers. Chapman and Hall.

Zaïri, F., Aour, B., Gloaguen, J.M., Naït-Abdelaziz, M., Lefebvre, J.M., 2008. Steady plastic flow of a polymer during equal channel angular extrusion process: Experiments and numerical modeling. Polym. Eng. Sci. 48, 1015–1021. https://doi.org/10.1002/pen.21042

Zaïri, F., Aour, B., Gloaguen, J.M., Naït-Abdelaziz, M., Lefebvre, J.M., 2007. Influence of the initial yield strain magnitude on the materials flow in equal-channel angular extrusion process. Scr. Mater. 56, 105–108. https://doi.org/10.1016/J.SCRIPTAMAT.2006.09.032

Zaïri, F., Aour, B., Gloaguen, J.M., Naït-Abdelaziz, M., Lefebvre, J.M., 2006. Numerical modelling of elastic–viscoplastic equal channel angular extrusion process of a polymer. Comput. Mater. Sci. 38, 202–216. https://doi.org/10.1016/J.COMMATSCI.2006.02.008

Zaïri, F., Naït-Abdelaziz, M., Gloaguen, J.M., Lefebvre, J.M., 2011. A physically-based constitutive model for anisotropic damage in rubber-toughened glassy polymers during finite deformation. Int. J. Plast. 27, 25–51. https://doi.org/10.1016/J.IJPLAS.2010.03.007

Zaïri, F., Naït-Abdelaziz, M., Gloaguen, J.M., Lefebvre, J.M., 2010. Constitutive modelling of the large inelastic deformation behaviour of rubber-toughened poly(methyl methacrylate): effects of strain rate, temperature and rubber-phase volume fraction. Model. Simul. Mater. Sci. Eng. 18, 055004. https://doi.org/10.1088/0965-0393/18/5/055004

Zaïri, F., Naït-Abdelaziz, M., Woznica, K., Gloaguen, J.-M., 2005a. Constitutive equations for the viscoplastic-damage behaviour of a rubber-modified polymer. Eur. J. Mech. - A/Solids 24, 169–182. https://doi.org/10.1016/J.EUROMECHSOL.2004.11.003

Zaïri, F., Woznica, K., Naït-Abdelaziz, M., 2005b. Phenomenological nonlinear modelling of glassy polymers. Comptes Rendus Mécanique 333, 359–364. https://doi.org/10.1016/J.CRME.2005.02.003

Zisman, A.A., Rybin, V.V., Van Boxel, S., Seefeldt, M., Verlinden, B., 2006. Equal channel angular drawing of aluminium sheet. Mater. Sci. Eng. A 427, 123–129. https://doi.org/10.1016/J.MSEA.2006.04.007